



THE UNIVERSITY *of* EDINBURGH

Edinburgh Research Explorer

Interactions of CO₂ with Formation Waters, Oil and Minerals and CO₂ storage at the Weyburn IEA EOR site, Saskatchewan, Canada

Citation for published version:

Hutcheon, I, Shevalier, M, Durocher, K, Bloch, J, Johnson, G, Nightingale, M & Mayer, B 2016, 'Interactions of CO₂ with Formation Waters, Oil and Minerals and CO₂ storage at the Weyburn IEA EOR site, Saskatchewan, Canada', *International Journal of Greenhouse Gas Control*.
<https://doi.org/10.1016/j.ijggc.2016.08.004>

Digital Object Identifier (DOI):

[10.1016/j.ijggc.2016.08.004](https://doi.org/10.1016/j.ijggc.2016.08.004)

Link:

[Link to publication record in Edinburgh Research Explorer](#)

Document Version:

Peer reviewed version

Published In:

International Journal of Greenhouse Gas Control

Publisher Rights Statement:

© 2016 Elsevier Ltd. All rights reserved.

General rights

Copyright for the publications made accessible via the Edinburgh Research Explorer is retained by the author(s) and / or other copyright owners and it is a condition of accessing these publications that users recognise and abide by the legal requirements associated with these rights.

Take down policy

The University of Edinburgh has made every reasonable effort to ensure that Edinburgh Research Explorer content complies with UK legislation. If you believe that the public display of this file breaches copyright please contact openaccess@ed.ac.uk providing details, and we will remove access to the work immediately and investigate your claim.



Interactions of CO₂ with Formation Waters, Oil and Minerals and CO₂ storage at the Weyburn IEA EOR site, Saskatchewan, Canada

Ian Hutcheon¹, Maurice Shevalier¹, Kyle Durocher¹, John Bloch², Gareth, Johnson³, Michael Nightingale¹ and Bernhard Mayer¹

¹Applied Geochemistry Group, Department of Geoscience, University of Calgary, Calgary, Alberta, Canada, T2N 1N4

²Guadalupita, New Mexico, USA

³School of Geosciences, University of Edinburgh, Edinburgh, United Kingdom, EH9 3FE

Abstract

The Weyburn oil field in Saskatchewan, Canada, is hosted in Mississippian carbonates and has been subject to injection of CO₂ since 2000. A detailed mineralogy study was completed as the basis for modeling of mineral storage of injected CO₂. Combining the mineralogy with kinetic reaction path models and water chemistry allows estimates of mineral storage of CO₂ over 50 years of injection. These results, combined with estimates of pore volume, solubility of CO₂ in oil and saline formation waters, and the initial and final pore volume saturation with respect to oil, saline water and gas/supercritical fluid allow an estimate of CO₂ stored in saline water, oil and minerals over 50 years of CO₂ injection. Most injected CO₂ is stored in oil ($6.5 \cdot 10^6$ to $1.3 \cdot 10^7$ tonnes), followed closely by storage in supercritical CO₂ ($7.2 \cdot 10^6$ tonnes) with saline formation water ($1.5 - 2 \cdot 10^6$ tonnes) and mineral storage ($2 - 6 \cdot 10^5$ tonnes) being the smallest sinks. If the mineral dawsonite forms, as modeling suggests, the majority of CO₂ dissolved in oil and saline formation water will be redistributed into minerals over a period of approximately 5000 years. The composition of produced fluids from a baseline sampling program, when compared to produced fluids taken three years after injection commenced, suggest that dawsonite is increasingly stable as pH decreases due to CO₂ injection. The results suggest that hydrocarbon reservoirs that contain low gravity oil and little or no initial gas saturation prior to CO₂ injection, may store the majority of injected CO₂ solubilized in oil, making such reservoirs the preferred targets for combined enhanced oil recovery-CO₂ storage projects.

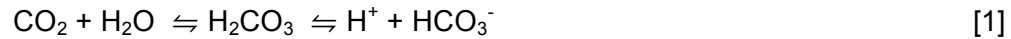
1. Introduction

Carbon capture and geological storage (CCS) is a promising technology for reducing CO₂ emissions into the atmosphere from fossil fuel intensive industries and energy production (Intergovernmental Panel on Climate Change (IPCC), 2005). There are over 200 enhanced oil recovery CO₂ injection projects in the United States and six in Canada as of 2015 (Verma, 2015). This technology has been piloted at various sites world-wide for more than 15 years and several full-scale storage projects have been established. As of December 2015, the Massachusetts Institute of Technology Carbon Capture and Sequestration technologies world-wide on-line database (sequestration.mit.edu) shows 22 power plant CCS projects, 33 non-power plant CCS projects, 9 commercial Enhanced Oil Recovery (EOR) projects, and 25 pilot CCS projects ranging from a few tonnes, to millions of tonnes, per year of injected CO₂. For all CO₂ injection sites, it is highly desirable to monitor the CO₂ plume distribution within the target reservoir and to verify the nature and amount of CO₂ storage in the reservoir, so as to demonstrate the conformance and safety of these operations.

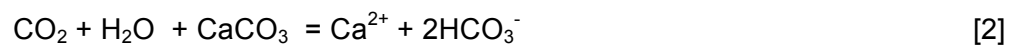
Storage of CO₂ in geological reservoirs may occur as supercritical fluid underneath the caprock, as residual trapping in pore spaces, solubility trapping in formation water, or mineral trapping. As outlined and predicted by the IPCC (2005), storage as supercritical fluid and via residual trapping are expected to be dominant in the early years of CO₂ storage projects. Solubility trapping in the formation waters is assumed to steadily increase in the medium term (e.g. decades). Mineral trapping of injected CO₂ has been suggested as a long-term process that may fix injected CO₂ on timelines of hundreds to thousands of years (IPCC, 2005), although faster rates of mineral trapping have been observed under favorable circumstances (Matter et al., 2016). Over the last few years, sufficient monitoring data have emerged from various CO₂ storage reservoirs to allow testing of the efficiency of CO₂ storage mechanisms and the associated time lines that are dependent on the reservoir.

The relative contributions of the various CO₂ storage mechanisms and their temporal evolution are critically dependent on whether CO₂ is injected into saline aquifers or whether CO₂ is used for enhanced oil recovery in mature oil fields such as Weyburn. Furthermore, the reservoir geology and mineralogy is of critical importance for assessing the reactions and reaction rates involved in geological CO₂ storage and sequestration (Gunter et al., 2004). Solubility trapping of injected CO₂ as in reaction [1] occurs as dissolved CO₂ in saline formation water as H₂CO₃, HCO₃⁻, and CO₃²⁻, depending on salinity and chemistry of the water and pressure and

temperature of the reservoir (Duan and Sun, 2003).



Ionic trapping takes place when the injected CO₂ lowers the pH of the formation water causing dissolution of carbonate minerals, such as calcite, as in reaction [2]. Half of the carbon in the bicarbonate in reaction [2] results from dissolution of CO₂, the other half from dissolution of carbonate minerals.



In a three week, single well “push-pull” CO₂ injection test into the contact between a dolerite sill and metamorphosed siltstones and mudstones, Assayag et al. (2009) observed that dissolution of carbonate minerals was the dominant mechanism to neutralize H₂CO₃, followed by cation exchange or dissolution of silicate minerals. A similar short-term (3 days) test of CO₂ injection in the Frio Formation, a fine grained quartz feldspar sandstone with minor amounts of illite, smectite and calcite showed calcite dissolution as the dominant reaction (Hovorka et al., 2006; Kharaka et al., 2006). Further sampling over an eight-month period showed increase in dissolved iron and, potentially increases in dissolved organics. Using the Frio data, a 1-D radial flow model for reactive transport shows that gas saturation decreases due to dissolution and the formation of carbonate minerals, with all the injected CO₂ ultimately sequestered as carbonates (Xu et al., 2010). Using carbon isotope ratios, Mayer et al. (2013) showed movement of injected CO₂ from injectors to producers, dissolution of CO₂ in reservoir saline waters, and ionic trapping of injected CO₂ in conjunction with dissolution of carbonate minerals (Shevalier et al., 2013) over a ten year period at the Weyburn IEA EOR site. In mature oil fields, dissolution of molecular CO₂ in oil is an additional possible pathway of solubility trapping. Due to the high solubility of CO₂ in many oils (Mungan 1981), enhanced oil recovery projects using CO₂ are likely to achieve elevated solubility trapping of CO₂ more rapidly than CO₂ storage projects in saline aquifers. At Weyburn, Perez et al. (2006) conclude that significant dissolution of CO₂ in oil took place over a three-year period.

The extent of mineral trapping is equally dependant on the type of reservoir in which CO₂ is injected. Carbonate reservoirs, typically containing Ca, Mg, and Fe-bearing carbonates are considered to have low mineral trapping potential as injected CO₂ results in low pH, causing

carbonate minerals to dissolve. In contrast, siliciclastic minerals may buffer pH (Hutcheon et al., 1993) and provide additional potential for storage of CO₂ in the mineral and/or aqueous phase by reactions with aluminous silicate minerals (Gunter et al., 2000). Numerical simulation of kinetic mineral trapping of CO₂ by Xu et al. (2004) shows a strong dependence on rock type, with mineral trapping being of the same order of magnitude as dissolution of CO₂ in saline formation waters. These authors also showed that carbonate accumulation may reduce porosity and permeability, ultimately affecting fluid flow. Reservoirs containing aluminosilicate mineral assemblages, including feldspar, mica, or clay minerals, among others, can result in precipitation of Ca-Mg-Fe carbonate minerals and, potentially, dawsonite (NaAlCO₃(OH)₂). Some studies dispute that dawsonite can form, or persist, during CO₂ injection (Hellevang et al., 2005, 2011, 2013). Worden (2006) has reported diagenetic dawsonite in the Triassic Lam Formation, Yemen. Up to 8 % (volume) dawsonite is observed and is interpreted to have formed between 85-100°C, preceding the growth of ferroan dolomite, and post-dating quartz. Some dawsonite is observed replacing plagioclase (albite) in perthite (plagioclase-potassium feldspar intergrowth). Dawsonite is reported as a diagenetic mineral from the Aldebaran Sandstone (Baker, 1991), Australia and is interpreted to have formed late in the burial history, or possibly at present. Present day temperatures range from 20-75°C. Dawsonite is also reported as a diagenetic mineral in Eastern Australia (Baker et al., 1995) and is interpreted as being formed due to seepage of magmatic CO₂ at temperatures between 30-75°C. Ferrini et al. (2003) report hydrothermal formation of dawsonite in a mineralogically complex dawsonite-realgar-orpiment hydrothermal deposit at Koran, Albania. The dawsonite is associated mainly with dolomitic wall rocks that contain ankerite and subordinate amounts of quartz and clay minerals, rather than the relatively lower porosity sandstone-shale wall rocks, due to greater porosity of the former. Irrespective of whether or not dawsonite forms during injection of CO₂, it appears that siliciclastic reservoirs are generally more favorable for mineral trapping of injected CO₂ than carbonate reservoirs, although the latter may also contain some potentially reactive silicate minerals. Hellevang et al. (2013, and references therein) summarize known natural occurrences of dawsonite and conclude that extensive formation of dawsonite is usually found in alkaline environments. Natural environments in China and Yemen with high pCO₂ and circum-neutral pH do exist and in at least two examples dawsonite has formed from replacement of Na-plagioclase (albite). Hellevang et al. (2013) also note high CO₂ zones in the North Sea, lacking in Na-plagioclase, that do not show dawsonite formation, in spite of dissolution of K-feldspar and calcite, likely resulting from kaolinite forming as K-feldspar dissolves, limiting availability of Al³⁺.

From the preceding discussion, it follows that each storage reservoir will retain injected CO₂ by a mixture of different mechanisms and over different timelines. Therefore, CO₂ storage mechanisms and associated timelines should be determined and predicted for each geological storage site separately, provided that sufficient information is available on the geology, mineralogy, fluid geochemistry, reaction rates, porosity, and the distribution of oil, saline water and gas, in the proposed storage reservoir. One of the major CO₂ storage projects where this is feasible is the IEA-GHG Weyburn-Midale CO₂ Monitoring and Storage project in Saskatchewan, Canada.

The objective of this paper is to determine the potential storage of CO₂ in individual flow units within the Midale beds of the Weyburn field in the Phase 1A area (Figure 1). The storage reservoirs considered for CO₂ are:

- newly formed minerals
- ionic species in solution in saline formation water
- CO₂ dissolved in oil
- CO₂ in a gas of mixed composition and/or a supercritical phase.

2. Study Area and Background

2.1 Geological Setting

The Weyburn Oil Field in southeastern Saskatchewan covers an area of 180 km² and produces oil from Mississippian carbonates of the Williston Basin (Burrowes, 2001). The field was discovered in 1954 and after various stages of primary and secondary production, the owner of the field (PanCanadian, subsequently EnCana and now Cenovus) began a CO₂ injection project in 2000 to determine the feasibility of improving oil recovery. An agreement between industry, government and academia coordinated by the Petroleum Technology Research Centre (based in Regina, Saskatchewan) and sponsored by the International Energy Agency Greenhouse Gas (IEA-GHG) Research and Development Program implemented a \$40 million (CAD) international research project to combine the enhanced recovery effort with a CO₂ storage project at Weyburn (Wilson and Monea, 2004). The overall objective of the Weyburn Project was to assess the technical and economic feasibility of CO₂ storage in geological formations, to develop tools to predict and verify CO₂ storage performance, and to build a set of best practice guidelines for such projects (Hitchon, 2012). An outline of all the research activities at Weyburn

is presented in White et al. (2009). The scope of the IEA GHG Weyburn Monitoring and Storage Project includes a detailed geological, petrophysical, hydrogeological, geophysical, and geochemical study of the reservoir, caprock, overburden and surrounding surface and subsurface region. While significant progress has been made on these objectives, so far a comprehensive CO₂ storage budget revealing the predominant CO₂ trapping mechanisms in the Weyburn field has not been provided.

Burrowes and Gilboy (2000) presented the geological setting of the Weyburn reservoir, and the distribution of flow units within the reservoir is described by Burrowes (2001). The Weyburn field is one of a number of large oilfields that lie along the Mississippian subcrop belt on the northern extent of the Williston Basin approximately 130 kilometers southeast of Regina, Saskatchewan. Medium gravity crude oil is produced from the Midale beds of the Mississippian Charles Formation. The location, stratigraphy and operational factors at Weyburn are presented in Shevalier et al. (2013). A detailed description of the lithofacies and depositional history of the Midale in southeastern Saskatchewan in the vicinity of the Weyburn field is presented by Qing and Nimegeers (2008). Regional hydrogeology and hydrogeochemistry for the Midale Fm., as well as the overlying Ratcliffe and underlying Frobisher Formations is detailed by Jensen et al. (2013).

A complete description of the stratigraphy and the geological position of the Marly and Vuggy flow units at Weyburn is given in Shevalier et al. (2013), and the following is a brief summary. The Weyburn reservoir is comprised of the tight dolomitic Marly zone and the underlying calcitic more permeable Vuggy Shoal, and less permeable Vuggy Intershoal zones, and is sealed by the Midale Evaporite anhydrite cap. Cenovus Ltd., the operator of the Weyburn field, has established a core-based, sequence stratigraphic interpretation of the Midale Marly and Midale Vuggy units (Figure 2 in Shevalier et al., 2013; Burrowes, 2001). Burrowes (2001) and Burrowes and Gilboy (2000) list general porosity and permeability estimates for the various flow units. The Midale Marly is characterized by high porosity (26%), and variable permeability (10 MD). The Midale Vuggy shoal has lower porosity (15%), but high permeability (50 MD), and the Vuggy intershoal unit is characterized by low porosity (10%) and low permeability (3 MD). Burrowes (2001) describes the Midale Vuggy as a heterogeneous calcareous, algal/coated-grain/pisolitic wackestone, packstone and grainstone with visible fenestral and vuggy porosity. The Marly is described as microsugrosic dolostone with mud dominant fabric. There is patchy cementation by calcite, anhydrite and dolomite. An examination of the potential effect of the petrology of the

Marly and Vuggy on mineral reactions and storage of CO₂ at Weyburn is presented by Durocher et al. (2003, 2005).

2.2 CO₂ Flood and Enhanced Oil Recovery

Injection of CO₂ improves oil recovery by lowering interfacial tension, swelling the oil, reducing viscosity and by mobilizing lighter components in the oil (Verma, 2015). Injection of CO₂ started at Weyburn in the fall of 2000 in the Phase 1A area, in the northwest corner of the Weyburn field. Early experimental studies outlined the mechanisms of CO₂ enhanced recovery (Holm, 1959). Correlations to determine miscibility of CO₂ with oil show a dependence on oil composition and density (API gravity) (Holm and Josendal, 1974; Mungan 1981). Oil density varies widely over the Weyburn field (Figure 1), thus solubility of CO₂ is expected to be variable. Srivastava and Huang (1997) and Srivastava et al. (2000) have measured the solubility of CO₂ in Weyburn reservoir oils. Sampling of oil from a single well at Weyburn over a ten year period shows dissolution of CO₂ in oil up to 38.5 mol percent (Yuo et al., 2013). A preliminary estimate for the entire Weyburn field suggests potential storage of up to 45.15 MT of CO₂, comprised of trapping by solubility (22.65 MT), ionic (0.25 MT) and equilibrium mineral storage (22.25 MT) mechanisms (Wilson and Monea, 2004). A detailed study of produced fluid compositions by Shevalier et al. (2013) confirms that CO₂ dissolution in saline water and subsequent reaction with calcite has taken place over a ten-year period of CO₂ injection at Weyburn. Shevalier et al. (2013) present the mechanisms and amounts of CO₂ stored in saline formation water by solubility and ionic trapping at Weyburn in Phase 1A. As of 2012, 22 million tonnes have been injected over the entire Weyburn field (Petroleum Technology Research Centre, 2014). Injection data since that date are not presently available.

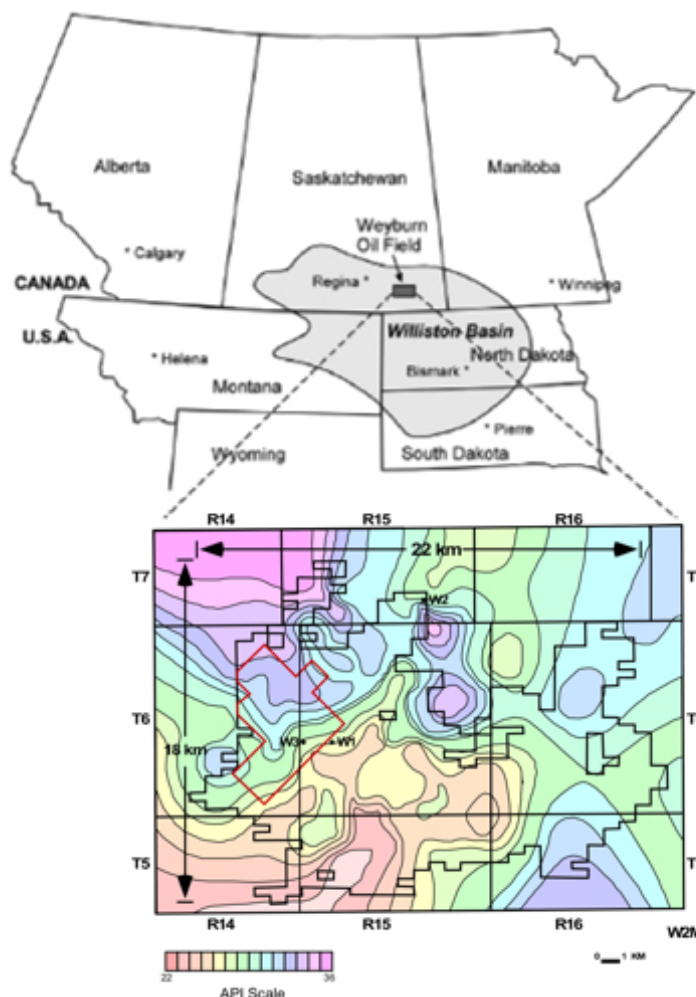


Figure 1. Location map of the Weyburn field in southern Saskatchewan, Canada. The phase 1A area is shown in the shaded area of the inset. The inset map of the Weyburn field is contoured for values of oil API gravity. W1, W2 and W3 are the locations of wells with measured solubility of CO₂ in oil from Srivastava et al. (2000).

3. Methodology

One hundred (100) core samples were obtained from the flow units described by Burrowes (2001). Cenovus supplied flow unit intervals (personal communication, Geoff Burrowes) and samples of drill core were selected to maximize the number of samples obtained from each flow unit. Cores were also selected to correlate with wells sampled for the geochemistry fluid/gas monitoring program that was conducted at Weyburn (Emberley et al., 2005; Raistrick et al., 2006; Shevalier et al., 2013). Five primary analytical methods were utilized: 1. Polished thin section examination by petrographic (PM) and scanning electron (SEM) microscopy to obtain general textural and mineralogical information. 2. X-Ray Diffraction (XRD) to provide mineral

identification and relative proportions. 3. X-Ray Fluorescence (XRF) and Inductively-Coupled Plasma Mass Spectrometry (ICP-MS) to obtain whole rock major and trace element composition, 4. Electron Probe Microanalysis (EPMA) for mineral identification and chemistry, and 5. Linear Programming Normative Analysis (LPNORM: Caritat et al., 1994) to produce quantitative mineralogy from the analytical results.

Textural information used to inform simulations was gathered by PM and SEM. XRD results show only the relative proportions of identifiable minerals, and not the absolute abundances. LPNORM (de Caritat et al., 1994) was used with XRD chemical analytical data (XRF, ICP-MS) to quantify the amounts and compositions of mineral phases. Whole rock geochemistry results are primary input for LPNORM, along with XRD estimates and electron probe microanalytical (EPMA) results. EPMA was used to identify oxides, sulfides, and clay-sized minerals in thin section, and to gather quantitative mineral composition data for LPNORM input. The computer code LPNORM (de Caritat et al., 1994) performs normative analysis from a bulk chemical analysis and from the composition of contained minerals. The user can specify the list of minerals and elemental oxides to be considered for normative analysis, and their composition (mineral formulae or geochemical compositions). LPNORM requires that the XRD data, bulk rock chemistry and the EPMA analyses of individual mineral grains are consistent with the calculated mineral mode. This combination of a number of methods, requiring that the total rock composition be consistent with the mineral modes and compositions, has an additional constraint (conservation of mass) compared to quantitative XRD analysis (e.g. Omotoso et al., 2006) alone.

The volumes of CO₂ stored as minerals, in saline formation water, as gas or supercritical fluid, and in oil were estimated for each flow unit. This was achieved as follows:

1. Mineralogical variations in flow units of the Phase 1A area of the Weyburn oilfield were determined.
2. Equilibrium rock-water reactions resulting from injection of CO₂, taking account of the solubility of CO₂ in saline water, were simulated. This step uses initial (pre CO₂ injection) conditions to provide the starting fluid composition for kinetic models. Simulations of total CO₂ injected to reach solubility of CO₂ in saline water identified potential mineralogical storage mechanisms and an estimate of maximum storage by mineral reactions.
3. Kinetic rock-water reactions during injection of CO₂, were simulated, taking account of

the solubility of CO₂ in saline water. The resulting amount of CO₂ stored is compared to an equilibrium model. This step approximates the storage by mass transfer, accounting for rates of dissolution and precipitation of the minerals identified in the previous step.

4. As dawsonite is an important potential contribution to mineral storage, limitations on its formation and the impact of dawsonite precipitation, or lack thereof, on storage of CO₂ were examined.
5. The relative amounts of CO₂ present stored as mineral phases, dissolved in saline formation water, dissolved in a gas (vapor) phase, and dissolved in oil at the end of CO₂ injection (after 50 years) are then estimated.

The steps involved in deriving the estimated relative amounts are:

1. The solubility of CO₂ in reservoir saline water at P-T is determined for each flow unit using two baseline water samples representing the range of TDS.
2. The reaction of CO₂, utilizing the formation mineralogy, is simulated using the REACT module of Geochemists Workbench® to calculate CO₂ storage at equilibrium due to CO₂ solubility in saline formation water and mineral reactions. The resulting CO₂ consumption is combined with the pore volume and pore saturation (oil-gas-saline water ratio) pre and post CO₂ injection of Marly and Vuggy flow units to determine an estimate of maximum CO₂ storage in saline water and minerals in the Phase 1A unit.
3. Kinetic models are evaluated for the same conditions as step 2 to determine the impact that reaction rates have on the amount of mineral storage.
4. A final audit of the amount of CO₂ stored is presented to evaluate the relative importance of SO₂ solubility in saline formation water and oil, the amount of supercritical CO₂, and the amount stored by mineral reactions, contrasting equilibrium and kinetic models.

Kinetic reaction path models in REACT use the same parameters as the equilibrium models, except rate constants (Palandri and Kharaka, 2004) and surface areas are included for the silicate minerals. The first step in the simulations is to equilibrate the mineralogy with the respective water, high or low TDS, at reservoir conditions (60°C and 170 bar). The resulting fluid composition is then used with the mineral amounts and reaction rate expressions to evaluate how much CO₂ is required to reach saturation in the saline formation water over the assumed

50 year injection period. The rates for carbonate minerals and anhydrite are not included in simulations as they react rapidly compared to the silicates.

The stability of dawsonite is examined by comparing the equilibrium stability field of dawsonite to the measured chemistry from produced water and gas samples. The equilibrium stability of dawsonite relative to albite, analcime, Na-beidellite and kaolinite was calculated using the ACT2 module of Geochemists Workbench®. The fugacity of CO₂ was determined from the baseline and Monitor 9 produced fluid compositions using the produced gas composition, reservoir temperature and pressure, and fugacity coefficients from Duan and Sun (2003). The activity of dissolved silica and the activity ratio of Na⁺/H⁺ was calculated using SOLMIN88 (Kharaka et al., 1988) with the pH (aH⁺) determined at reservoir conditions by the methods outlined in Shevalier et al (2013).

4. Analytical Results

4.1 Mineralogy of Storage Reservoir Flow Units

The mineralogy results are too extensive to be presented here, however they are available as supplemental material. Summary results by flow unit that combine all PM, SEM, XRD, XRF, ICP-MS, EPM data with the average of LPNORM calculated modes, normalized to 100%, are presented in Table 1.

Table 1. Average LPNORM Mineralogy for Weyburn Reservoir Samples (93). Normalized to 100 wt %

| Unit | samples | Flow Unit | Calcite | Dolomite | Anhydrite | Quartz | K-Feldspar | Plagioclase | Illite | Kaolinite | Anatase | Apatite |
|-------------------------------------|---------|-----------|---------|----------|-----------|--------|------------|-------------|--------|-----------|---------|---------|
| Midale Evaporite-Three Fingers Zone | 8 | ME-TF | 0.7 | 60.0 | 5.3 | 16.8 | 9.1 | 3.0 | 4.7 | 0.0 | 0.3 | 0.0 |
| Midale Marly | 11 | M0 | 11.7 | 65.9 | 6.3 | 7.4 | 4.9 | 1.6 | 2.2 | 0.0 | 0.1 | 0.0 |
| Midale Marly | 4 | M1 | 24.4 | 47.9 | 20.2 | 3.6 | 2.7 | 1.0 | 0.1 | 0.0 | 0.1 | 0.0 |
| Midale Marly | 15 | M3 | 21.8 | 62.7 | 5.2 | 4.6 | 3.5 | 1.3 | 0.7 | 0.2 | 0.1 | 0.0 |
| Midale Vuggy | 7 | V1 | 82.3 | 11.6 | 2.8 | 1.5 | 0.9 | 0.6 | 0.3 | 0.0 | 0.0 | 0.0 |
| Midale Vuggy | 12 | V2 | 89.9 | 5.0 | 3.6 | 0.7 | 0.3 | 0.4 | 0.0 | 0.0 | 0.0 | 0.0 |
| Midale Vuggy | 6 | V3 | 76.7 | 16.1 | 2.5 | 2.2 | 1.5 | 0.8 | 0.0 | 0.0 | 0.0 | 0.0 |
| Midale Vuggy | 12 | V4 | 77.5 | 13.3 | 3.3 | 2.2 | 2.0 | 0.9 | 0.7 | 0.1 | 0.1 | 0.0 |
| Midale Vuggy | 6 | V6 | 68.8 | 14.6 | 12.8 | 1.8 | 0.5 | 0.3 | 0.2 | 0.9 | 0.0 | 0.0 |
| Frobisher Marly | 10 | FM | 4.5 | 72.7 | 8.1 | 6.9 | 4.4 | 2.0 | 1.3 | 0.0 | 0.1 | 0.1 |
| Frobisher Evaporite | 2 | FE | 23.5 | 15.9 | 59.1 | 0.8 | 0.4 | 0.3 | 0.0 | 0.0 | 0.0 | 0.0 |

The most commonly found minerals include dolomite, calcite and trace amounts of ankerite (in Marly units of the Midale and Frobisher), calcite (dominantly in Vuggy units), and anhydrite (all units to some degree). Silicate minerals quartz, mica (illite) and K-feldspar are also present, and tend to be more common in the Marly flow units. Trace amounts of celestite, illite, and gypsum were identified. Although pyrite and fluorite were found in trace amounts in most samples (EPMA), these minerals were not easily identifiable in XRD traces due to low abundance. K-feldspar was found in virtually all samples using the electron microprobe, but was identified in only some reservoir samples using XRD. These observations suggest that XRD mineral identification is limited to phases in excess of several volume percent.

Oxide totals for all samples are highly variable and range between 40 and 90 wt.%. The average oxide total is approximately 70%. The high loss on ignition (LOI) may be due to bitumen and water. Samples that are dominantly calcite (Vuggy) have CaO contents that approach 56 wt.%. Dolomitic samples (Marly) have elevated MgO contents (up to 20 wt.%).

Silicate-rich samples (Marly) have higher SiO₂, Al₂O₃, and K₂O contents (up to 50, 7, and 4 wt.%, respectively), while samples with significant amounts of anhydrite and celestite (Vuggy) have elevated S, Sr, and Ba values (up to 350,000, 35,000, and 700 ppm, respectively).

EPMA images and some observations are shown in representative summary Figures 2 and 3. Several mineral phases were observable using EPMA that were not observed using microscopic or XRD examination. The most commonly found trace mineral phases (< 3 vol%) are K-feldspar, illite, fluorite, and pyrite. Less commonly found minerals (< 1 vol%) include celestite, apatite, anatase, zircon, hematite, pyrrhotite, and chalcopyrite. Calcite and dolomite from reservoir samples were near the stoichiometric composition (suggesting ordered dolomite), with minor and variable amounts of SrO, FeO, and MnO. K-feldspar contained variable amounts of Na₂O and CaO, potentially reactive elements during silicate-CO₂ reactions in the presence of pore fluids. Illite grains were typically smaller than 20 µm in length, and were generally too small to analyze quantitatively.

Petrography, LPNORM Results and Flow Unit Properties

For the purposes of simulations of the water-rock reactions that take place during injection of CO₂, it is necessary to have data on the mineralogy, texture, porosity and pore volume of each flow unit. Cenovus (G. Burrowes; personal communication) provided the porosity and pore volume for each of the flow units.

The petrography, including thin section and backscattered electron photomicrography, is combined in the following descriptions of individual flow units. Also, the normative calculations, along with information that is either used to constrain the LPNORM calculation, or to interpret the results, are presented. Only representative data for the Midale Marly and Midale Vuggy, the most volumetrically significant units in the Weyburn Field, are presented here, although all units, including bounding units above and below the Midale, were examined. In the following discussion, all mineral modes are presented as weight percent. Carbonate rock classification is according to Dunham (1962).

Midale Marly

The Midale Marly is a dolomite-dominated series of units (M0, M1, & M3; Burrowes, 2001; Shevalier et al., 2013, Figure 2) characterized by finely crystalline dolomite (50-65%) and silicates. Rocks are dominantly mudstone to wackestone (finely crystalline dolomite to

biomicrite). Dolomite grains are typically <20 µm in diameter, with some samples displaying planar-porphyrotopic dolomite rhombs up to 100 µm in diameter. All units are either massive and structureless, or thinly laminated, with alternating zones of dolomite- and silicate-dominant layers. Porosity is generally submicroscopic to pinpoint (<100 µm), subrounded, and clear of secondary mineralization. Downward through the stratigraphic section, toward the Midale Vuggy units, calcite is more commonly found, with mixed skeletal fragments, anhydrite pore filling, and anhydritization. Bitumen is common throughout the Midale Marly.

There are three flow units, M0, M1 and M3 identified in the Midale Marly. The M2 is a low porosity calcareous marker (Burrowes, 2001) and is not considered further. Calcite is less common than in the Midale Vuggy units, but is still significant (10-25 wt%), with anhydritization common only in the M1 flow unit (20 wt%). The Midale Marly has the greatest amount of silicate minerals (7.5-16 wt%) of all the reservoir flow units, with quartz being the most common silicate. Trace feldspar and illite (approximately 50 wt% of the silicate minerals present) are more commonly found within the Marly than the Vuggy shoal and intershoal. LPNORM results suggest plagioclase feldspar is dominantly comprised of the albite (Na) component. **Figure 2** shows representative views of the M0, which is broadly similar to the M1 and M3 flow units.

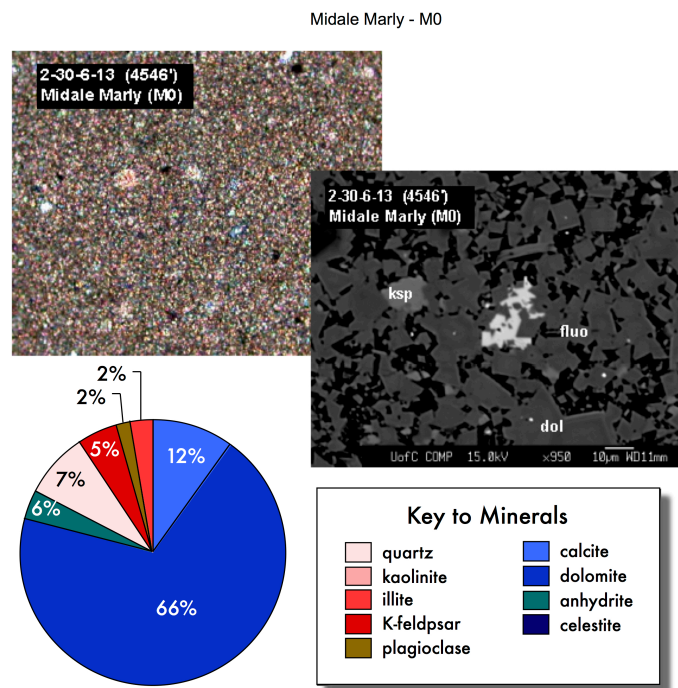


Figure 2. Representative petrography and mineral abundance data for the Midale Marly M0 flow unit. Thin section field of view is 500 μm . Scale bar on the SEM photomicrograph is 10 μm .

Midale Vuggy

The Midale Vuggy intershoal is a highly variable collection of rock types that range from microcrystalline calcitic (micrite) mudstone to packstone (intramicrite, dismicrite, and biomicrite common). V1 flow unit has small to submicroscopic pores ($<100\ \mu\text{m}$) that are subrounded to rounded, and largely unfilled although some calcite pore filling is observed. Planar-porphyrrotopic dolomite growth is common, as is anhydritization of micrite. Bitumen layers are common, most often associated with coarser crystalline silicate-rich layers. Skeletal fragments are also observed.

The Midale Vuggy shoal is highly variable in the range of rock types, but also is micritic. Dominated by wackestone (biomicrite), these units have large, irregularly shaped pores (up to 2 mm diameter), partially filled with calcite, dolomite, and anhydrite. Bioclasts (brachiopod shells, ooids) are rare to common, as is nodular calcite and celestite. Anhydritization of matrix calcite is most commonly found at the base of the Vuggy shoal. The lowermost unit immediately overlies an erosional contact with the Frobisher Marly and Frobisher Evaporite. Compaction features such as stylolites, elongated pelloidal calcite, and skeletal grains are found in all Vuggy shoal units.

Five Midale Vuggy flow units were identified by Burrowes (2001), V1, the intershoal unit and the shoal units V2, V3, V4 and V6. Our results show the Midale Vuggy flow units are dominated by calcite (70-90%), relatively minor amounts of dolomite (5-15 wt%) and traces of anhydritization (3-13 wt%). Vuggy flow unit V6, immediately above the Frobisher erosion surface, contains variable but significant anhydrite (13 wt%). Silicate minerals in the Midale Vuggy are found in minor to trace amounts (2-15 wt%). Quartz comprises approximately 50 wt% of the silicate minerals with lesser amounts of plagioclase (albite) and illite. The Midale Vuggy has lower porosity than the Midale Marly, but the pore structure of the Vuggy has allowed more oil, prior to CO_2 injection, to be removed proportionally from the Vuggy than the Marly. **Figure 3** shows representative data for the V2. The V1, V3, V4, and V6 flow units are broadly similar.

Midale Vuggy - V2

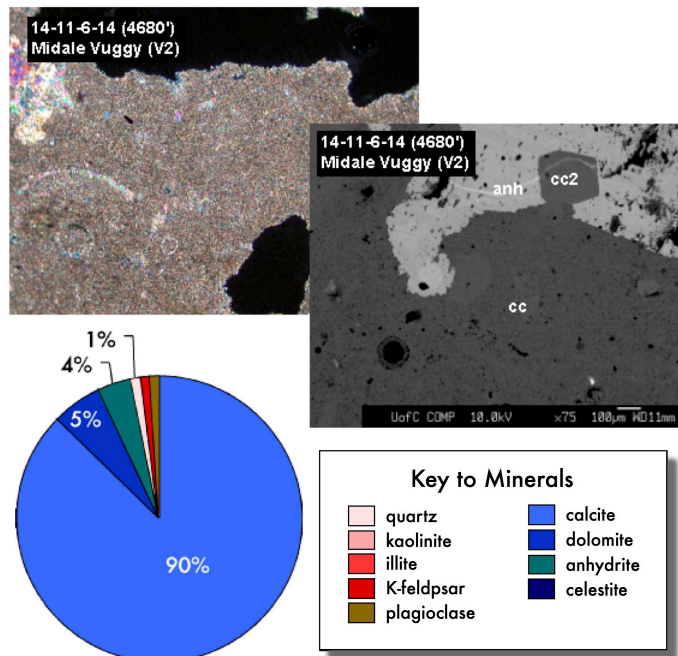


Figure 3. Representative petrography and mineral abundance data for the Midale Vuggy V2 flow unit. Thin section field of view is 500 μm . Scale bar on the SEM photomicrograph is 100 μm .

The Midale Evaporite Three Fingers Zone represents the top reservoir seal. It has low porosity and permeability (not measured) and is comprised dominantly of carbonate minerals and anhydrite with significant amounts of K-feldspar, illite and plagioclase. The Midale Marly (M0, M1, M3 flow units) is the target for improved oil recovery as it has, prior to CO_2 injection, the highest oil saturations. These units have high porosity, approximately 20 volume % on average, are dominated by dolomite, and contain 10-20 wt% calcite and minor amounts of quartz with traces (less than 5 wt%) of K-feldspar and plagioclase (albite). The M1 and M3 contain the greatest pore volume (77% of pore volume) in the Midale Marly. The Midale Vuggy has lower oil saturations prior to CO_2 injection, and lower porosity (7-10 volume %). It is dominated by calcite, with 5-15 wt% dolomite and minor amounts of quartz. There are lesser amounts of K-feldspar (0.4-4.9 wt%) and plagioclase (0.3-2.0 wt%) that LPNORM results show to be albite composition. The V1 and V2 flow units account for the majority (60 volume%) of the pore volume.

4.2 Geochemistry of Formation Water and Residual Oil

The Weyburn Phase 1A area shows considerable variation in fluid composition within the Midale (Emberley et al., 2005), therefore a high total dissolved solids (TDS) and low TDS sample were selected from Baseline samples collected in August 2000 at Weyburn (Emberley et al., 2005). Well 101/14-30-006-13W2 (47787 mg/l TDS) was selected as the low TDS (referred to as “Lo TDS” on subsequent figures) sample with a calculated equivalent salinity of 0.83 M. Well 141/14-07-006-13W2 (95123 mg/l TDS) was selected as the high TDS sample (referred to as “Hi TDS” on subsequent figures) and has a calculated equivalent salinity of 1.67 M. To examine the stability of dawsonite, the baseline water and gas compositions are compared to compositions from data during monitoring sample trip 9 (Monitor Trip 9, abbreviated M9 hereafter) collected in September 2003, three years after CO₂ injection began. Fluid compositions used in this paper are presented in Table 2.

Table 2. Geochemical compositions of produced water from Weyburn Phase 1A.

| Baseline Water Compositions - August 2000 (dots represent data not measured) | | | | | | | | | | | | | | | | |
|--|-------------|-------------|----------|--------|------------|-----------------|--------|--------|--------|--------|--------|------------------|--------|--------|-----------------|-----------------|
| DLS LOCATION | Reservoir T | Reservoir P | pH | pH | Alkalinity | S ²⁻ | Na | K | Ca | Mg | Sr | SiO ₂ | Cl | Br | SO ₄ | CO ₂ |
| (°C) | (bars) | | Downhole | (mg/L) | (ppm) | (mg/L) | (mg/L) | (mg/L) | (mg/L) | (mg/L) | (mg/L) | (mg/L) | (mg/L) | (mg/L) | (mg/L) | (mole %) |
| 101/02-10-006-14W2 | 52 | 140 | 6.61 | 6.29 | 578.5 | 203.7 | 26070 | 268.9 | 1158 | 366.2 | 65.19 | 26.53 | 44100 | 3850 | 3850 | 5.18 |
| 101/02-12-006-14W2 | 55 | 195 | 6.49 | 6.2 | 414.6 | 100.2 | 18960 | 382.3 | 1530 | 380.2 | 68.97 | 29.05 | 30025 | 74.0 | 3625 | 3.38 |
| 101/02-23-006-14W2 | 57 | 185 | 6.81 | 6.32 | 605.1 | 354.3 | 22560 | 364.6 | 1141 | 337.8 | 29.18 | 19.23 | 33960 | 64.0 | 3330 | 6.30 |
| 101/02-24-006-14W2 | 56 | 200 | 6.94 | 6.43 | 476.6 | 88.8 | 25070 | 434.5 | 1318 | 346.5 | 31.95 | 41.31 | 37555 | 56.0 | 3485 | 3.19 |
| 101/02-26-006-14W2 | 57 | 195 | 6.43 | 6.28 | 439.0 | 273.6 | 20700 | 488.4 | 1495 | 387.7 | 80.61 | 40.33 | 34250 | 66.5 | 3330 | 4.40 |
| 101/02-30-006-13W2 | 58 | 160 | 6.85 | 6.22 | 389.3 | 117.8 | 22510 | 123.5 | 1138 | 365.4 | 24.47 | 29.97 | 34960 | 59.0 | 3445 | 6.05 |
| 101/05-36-006-14W2 | 56 | 150 | 6.93 | 6.44 | 302.9 | 25.0 | 19820 | 162.9 | 1049 | 348.3 | 27.64 | 29.27 | 30225 | 53.0 | 3465 | 1.47 |
| 101/08-13-006-14W2 | 56 | 202.5 | 6.73 | 6.08 | 407.3 | 40.7 | 35860 | 427.9 | 1452 | 399.3 | 79.38 | 36.24 | 51720 | 72.5 | 3455 | 4.86 |
| 101/08-19-006-13W2 | 58 | 155 | 7.00 | 6.21 | 335.9 | 13.4 | 23020 | 389.7 | 1195 | 317.9 | 29.01 | 23.90 | 34320 | 47.5 | 3360 | 4.32 |
| 101/08-20-006-13W2 | 58 | 150 | 6.20 | 5.81 | 342.9 | 90.2 | 27580 | 365.4 | 1476 | 390.9 | 43.31 | 32.35 | 39545 | 71.0 | 3395 | 4.07 |
| 101/08-25-006-14W2 | 56 | 162.5 | 6.92 | 6.44 | 353.1 | 45.5 | 12220 | 128.4 | 1008 | 315.7 | 42.00 | 35.62 | 20635 | 44.5 | 3685 | 2.00 |
| 101/08-30-006-13W2 | 59 | 145 | 6.92 | 6.96 | 510.9 | 35.2 | 21500 | 218.4 | 1178 | 351.1 | 89.01 | 27.04 | 31745 | 57.5 | 3065 | 0.90 |
| 101/08-36-006-14W2 | 56 | 165 | 7.30 | 7.08 | 264.8 | 23.5 | 19940 | 345.7 | 1416 | 373.2 | 88.50 | 39.19 | 30815 | 60.0 | 3670 | 0.30 |
| 101/10-17-006-13W2 | 57 | 150 | 6.58 | 6.12 | 390.0 | 19.1 | 34180 | 584.9 | 1504 | 402.2 | 39.26 | 25.24 | 51200 | 73.5 | 3790 | 3.12 |
| 101/11-01-006-14W2 | 55 | 170 | 6.64 | 5.78 | 66.3 | 87.4 | 28710 | 400.4 | 1647 | 398.1 | 36.27 | 23.47 | 44000 | 70.5 | 3665 | 2.47 |
| 101/12-11-006-14W2 | 54 | 195 | 6.47 | 6.11 | 537.8 | 169.3 | 24570 | 269.0 | 1296 | 368.9 | 45.65 | 41.14 | 37855 | 67.0 | 3900 | 6.21 |
| 101/12-18-006-13W2 | 57 | 201 | 7.08 | 6.29 | 437.9 | 60.8 | 21540 | 359.6 | 1138 | 314.2 | 23.22 | 21.37 | 31645 | 51.5 | 3755 | 5.59 |
| 101/12-20-006-13W2 | 57 | 160 | 6.63 | 5.83 | 298.6 | 67.0 | 30070 | 558.9 | 1432 | 339.7 | 37.51 | 24.28 | 45480 | 65.5 | 3690 | 4.37 |
| 101/12-23-006-14W2 | 58 | 192.5 | 6.76 | 6.38 | 864.6 | 686.2 | 13770 | 225.2 | 945 | 421.1 | 15.43 | 52.35 | 19665 | 39.5 | 3665 | 1.28 |
| 101/12-25-006-14W2 | 55 | 202.5 | 6.75 | 6.7 | 519.8 | 284.2 | 14990 | 143.9 | 1122 | 346.3 | 31.40 | 38.64 | 24150 | 54.0 | 3695 | 4.28 |
| 101/12-26-006-14W2 | 60 | 155 | 6.79 | 6.64 | 550.4 | 283.9 | 22100 | 193.5 | 1166 | 335.5 | 86.96 | 19.79 | 32610 | 45.5 | 2995 | 0.61 |
| 101/14-01-006-14W2 | 54 | 140 | 6.34 | 5.8 | 493.4 | 121.6 | 40850 | 588.7 | 1319 | 411.5 | 44.38 | 14.68 | 60565 | 95.5 | 3105 | 4.57 |
| 101/14-02-006-14W2 | 52 | 197.5 | 6.78 | 6.28 | 232.7 | 77.5 | 29630 | 611.2 | 1592 | 415.1 | 41.42 | 23.55 | 43875 | 70.5 | 3565 | 2.03 |
| 101/14-23-006-14W2 | 60 | 162.5 | 6.40 | 6.3 | 704.2 | 133.5 | 11280 | 181.4 | 1110 | 327.9 | 62.89 | 24.13 | 19650 | 38.5 | 3680 | 3.62 |
| 101/14-30-006-13W2 | 56 | 150 | 6.88 | 6.84 | 359.3 | 52.6 | 16140 | 107.4 | 1096 | 325.5 | 60.26 | 31.88 | 26000 | 52.0 | 3065 | 6.04 |
| 121/02-13-006-14W2 | 58 | 190 | 6.68 | 5.15 | 398.3 | 145.6 | 22890 | 565.4 | 1687 | 399.1 | 92.56 | 26.68 | 35495 | 66.5 | 3440 | 2.83 |
| 121/08-17-006-13W2 | 58 | 152.5 | 6.50 | 5.63 | 277.0 | 66.1 | 35410 | 710.3 | 1696 | 439.0 | 44.22 | 37.01 | 55830 | 91.0 | 2895 | 4.22 |
| 121/08-18-006-13W2 | 55 | 165 | 6.45 | 6.26 | 395.8 | 168.2 | 29740 | 363.7 | 1571 | 385.5 | 40.71 | 38.66 | 44920 | 69.5 | 3405 | 3.08 |
| 121/13-18-006-13W2 | 55 | 197.5 | 6.57 | 6.2 | 367.0 | 152.4 | 30660 | 395.6 | 1782 | 457.1 | 46.70 | 15.85 | 43705 | 68.0 | 3600 | 3.32 |
| 121/14-08-006-13W2 | 52 | 170 | 6.88 | 6.11 | 391.1 | 34.6 | 35000 | 451.8 | 1388 | 374.5 | 62.02 | 27.19 | 47200 | 73.5 | 3265 | 4.47 |
| 121/14-13-006-14W2 | 52 | 112.5 | 6.62 | 6.27 | 422.0 | 52.8 | 27040 | 294.4 | 1399 | 378.1 | 53.06 | 19.57 | 39440 | 61.0 | 3440 | 4.16 |
| 141/08-07-006-13W2 | 58 | 165 | 6.57 | 6.01 | 358.8 | 123.6 | 27730 | 337.3 | 1559 | 390.8 | 84.07 | 22.08 | 42315 | 74.5 | 3680 | 4.22 |
| 141/08-12-006-14W2 | 56 | 210 | 6.79 | 6.35 | 386.9 | 49.3 | 29550 | 584.1 | 1615 | 371.1 | 39.39 | 19.75 | 46375 | 72.5 | 3675 | 4.12 |
| 141/08-23-006-14W2 | 58 | 155 | 7.00 | 6.55 | 470.7 | 188.6 | 24750 | 404.0 | 1359 | 381.5 | 39.11 | 25.65 | 38880 | 52.0 | 3320 | 2.48 |
| 141/14-06-006-13W2 | 56 | 100 | 6.84 | 6.42 | 710.5 | 17.2 | 29730 | 322.7 | 1373 | 425.8 | 31.76 | 29.35 | 51800 | 96.5 | 3040 | 3.98 |
| 141/14-07-006-13W2 | 56 | 135 | 6.85 | 6.09 | 371.6 | 138.4 | 34990 | 746.1 | 1552 | 395.1 | 45.70 | 25.63 | 53400 | 80.0 | 3160 | 4.46 |
| 141/14-11-006-14W2 | 53 | 115 | 6.50 | 5.9 | 389.3 | 103.5 | 29200 | 512.7 | 1760 | 387.0 | 35.64 | 22.91 | 45000 | 71.0 | 3175 | 9.69 |
| 141/14-18-006-13W2 | 55 | 210 | 6.31 | 6.05 | 437.1 | 182.9 | 19920 | 393.0 | 1238 | 363.8 | 79.68 | 25.59 | 32875 | 56.5 | 3850 | 5.25 |

Table 2. Geochemical compositions of produced water from Weyburn Phase 1A.

| Baseline Water Compositions - August 2000 (dots represent data not measured) | | | | | | | | | | | | | | | S ²⁻ | Na | K | Ca | Mg | Sr | SiO ₂ | Cl | Br | SO ₄ | CO ₂ |
|--|-------------|-------------|------|------|------------|----------|--------|-------|--------|--------|--------|--------|--------|--------|-----------------|----|---|----|----|----|------------------|----|----|-----------------|-----------------|
| DLS LOCATION | Reservoir T | Reservoir P | pH | pH | Alkalinity | Downhole | (mg/L) | (ppm) | (mg/L) | (mg/L) | (mg/L) | (mg/L) | (mg/L) | (mg/L) | | | | | | | | | | | |
| 101/02-10-006-14W2 | 52 | 140 | 6.61 | 6.29 | 578.5 | 203.7 | 26070 | 268.9 | 1158 | 366.2 | 65.19 | 26.53 | 44100 | 3850 | | | | | | | | | | | 5.18 |
| 101/02-12-006-14W2 | 55 | 195 | 6.49 | 6.2 | 414.6 | 100.2 | 18960 | 382.3 | 1530 | 380.2 | 68.97 | 29.05 | 30025 | 74.0 | | | | | | | | | | | 3.38 |
| 101/02-23-006-14W2 | 57 | 185 | 6.81 | 6.32 | 605.1 | 354.3 | 22560 | 364.6 | 1141 | 337.8 | 29.18 | 19.23 | 33960 | 46.0 | | | | | | | | | | | 6.00 |
| 101/02-24-006-14W2 | 56 | 200 | 6.94 | 6.43 | 476.6 | 88.8 | 25070 | 434.5 | 1318 | 346.5 | 31.95 | 41.31 | 37555 | 56.0 | | | | | | | | | | | 3.19 |
| 101/02-26-006-14W2 | 57 | 195 | 6.43 | 6.28 | 430.0 | 273.6 | 20700 | 488.4 | 1495 | 387.7 | 80.61 | 40.33 | 34250 | 66.5 | | | | | | | | | | | 4.05 |
| 101/02-30-006-13W2 | 58 | 160 | 6.85 | 6.22 | 388.3 | 117.8 | 22510 | 123.5 | 1138 | 365.4 | 24.47 | 29.97 | 34960 | 59.0 | | | | | | | | | | | 6.47 |
| 101/05-36-006-14W2 | 56 | 150 | 6.93 | 6.44 | 302.9 | 25.0 | 19520 | 162.9 | 1049 | 348.3 | 27.64 | 29.27 | 30225 | 53.0 | | | | | | | | | | | 1.47 |
| 101/08-13-006-14W2 | 56 | 202.5 | 6.73 | 6.08 | 407.3 | 40.7 | 35860 | 427.9 | 1452 | 399.3 | 79.38 | 36.24 | 51720 | 72.5 | | | | | | | | | | | 4.86 |
| 101/08-19-006-13W2 | 58 | 155 | 7.00 | 6.21 | 335.9 | 13.4 | 23020 | 389.7 | 1195 | 317.9 | 29.01 | 23.90 | 34320 | 47.5 | | | | | | | | | | | 4.32 |
| 101/08-20-006-13W2 | 58 | 150 | 6.20 | 5.81 | 342.9 | 90.2 | 27580 | 365.4 | 1476 | 390.9 | 43.31 | 32.35 | 39545 | 71.0 | | | | | | | | | | | 4.08 |
| 101/08-25-006-14W2 | 56 | 162.5 | 6.92 | 6.44 | 353.1 | 45.5 | 12220 | 128.4 | 1008 | 315.7 | 42.00 | 35.62 | 20635 | 44.5 | | | | | | | | | | | 2.92 |
| 101/08-30-006-13W2 | 59 | 145 | 6.92 | 6.96 | 510.9 | 35.2 | 21500 | 218.4 | 1178 | 351.1 | 89.01 | 27.04 | 31745 | 57.5 | | | | | | | | | | | 0.90 |
| 101/08-36-006-14W2 | 56 | 165 | 7.30 | 7.08 | 264.8 | 23.5 | 19940 | 345.7 | 1416 | 373.2 | 88.50 | 36.19 | 30815 | 60.0 | | | | | | | | | | | 0.36 |
| 101/10-17-006-13W2 | 57 | 150 | 6.58 | 6.12 | 390.0 | 18.1 | 34180 | 594.9 | 1504 | 402.2 | 39.26 | 25.24 | 51200 | 73.5 | | | | | | | | | | | 3.12 |
| 101/11-01-006-14W2 | 25 | 170 | 6.64 | 5.76 | 66.3 | 87.4 | 28710 | 400.4 | 1647 | 398.1 | 36.27 | 23.53 | 44100 | 70.5 | | | | | | | | | | | 2.47 |
| 101/12-11-006-14W2 | 54 | 195 | 6.47 | 6.11 | 537.8 | 169.3 | 24570 | 269.0 | 1296 | 368.9 | 45.65 | 41.14 | 37855 | 67.0 | | | | | | | | | | | 6.21 |
| 101/12-19-006-13W2 | 57 | 201 | 7.08 | 6.29 | 437.9 | 60.8 | 21540 | 359.6 | 1138 | 314.2 | 23.22 | 21.37 | 31645 | 51.5 | | | | | | | | | | | 5.59 |
| 101/12-20-006-13W2 | 57 | 160 | 6.63 | 5.83 | 296.6 | 67.0 | 30070 | 558.9 | 1432 | 339.7 | 37.51 | 24.28 | 45480 | 65.5 | | | | | | | | | | | 4.37 |
| 101/12-23-006-14W2 | 58 | 192.5 | 6.76 | 6.38 | 864.6 | 686.2 | 13770 | 225.2 | 945 | 421.1 | 15.43 | 52.35 | 19665 | 39.5 | | | | | | | | | | | 9.40 |
| 101/12-25-006-14W2 | 55 | 202.5 | 6.75 | 6.7 | 519.8 | 284.2 | 14990 | 143.9 | 1122 | 346.3 | 31.40 | 38.64 | 24150 | 54.0 | | | | | | | | | | | 1.28 |
| 101/12-26-006-14W2 | 60 | 155 | 6.79 | 6.64 | 550.4 | 283.9 | 22100 | 193.5 | 1168 | 335.5 | 86.96 | 19.79 | 32610 | 45.5 | | | | | | | | | | | 0.61 |
| 101/14-01-006-14W2 | 54 | 140 | 6.34 | 5.8 | 493.4 | 121.8 | 40850 | 588.7 | 1319 | 411.5 | 44.38 | 14.68 | 60565 | 95.5 | | | | | | | | | | | 4.57 |
| 101/14-02-006-14W2 | 52 | 197.5 | 6.78 | 6.28 | 232.7 | 77.5 | 29630 | 611.2 | 1592 | 415.1 | 41.42 | 23.55 | 43875 | 70.5 | | | | | | | | | | | 2.03 |
| 101/14-12-006-14W2 | 55 | 165 | 6.81 | 6.38 | 419.6 | 144.5 | 21720 | 552.4 | 1539 | 382.1 | 76.28 | 31.64 | 36710 | 69.5 | | | | | | | | | | | 3.62 |
| 101/14-14-006-14W2 | 54 | 90 | 6.77 | 6.25 | 602.1 | 44.7 | 24830 | 298.1 | 1402 | 398.3 | 30.05 | 15.96 | 36570 | 52.5 | | | | | | | | | | | 6.04 |
| 101/14-20-006-13W2 | 58 | 206 | 6.66 | 5.92 | 308.3 | 69.2 | 25030 | 400.4 | 1406 | 361.6 | 53.35 | 29.03 | 37000 | 68.5 | | | | | | | | | | | 4.14 |
| 101/14-23-006-14W2 | 60 | 162.5 | 6.40 | 6.3 | 704.2 | 133.5 | 11280 | 181.4 | 1110 | 327.9 | 62.89 | 24.13 | 19650 | 38.5 | | | | | | | | | | | 5.86 |
| 101/14-30-006-13W2 | 56 | 150 | 6.88 | 6.84 | 359.3 | 52.6 | 16140 | 107.4 | 1096 | 325.5 | 60.26 | 31.88 | 26000 | 52.0 | | | | | | | | | | | 0.87 |
| 121/02-13-006-14W2 | 58 | 190 | 6.88 | 5.15 | 398.3 | 145.6 | 22890 | 565.1 | 1687 | 399.1 | 92.56 | 26.68 | 35495 | 66.5 | | | | | | | | | | | 4.22 |
| 121/08-17-006-13W2 | 58 | 152.5 | 6.50 | 5.63 | 277.0 | 66.1 | 35410 | 710.3 | 1696 | 439.0 | 44.22 | 37.01 | 55830 | 91.0 | | | | | | | | | | | 2.83 |
| 121/08-18-006-13W2 | 55 | 165 | 6.45 | 6.26 | 395.8 | 168.2 | 29740 | 363.7 | 1571 | 385.5 | 40.71 | 38.66 | 44920 | 69.5 | | | | | | | | | | | 3.00 |
| 121/13-18-006-13W2 | 35 | 197.5 | 6.57 | 6.2 | 367.0 | 152.4 | 30660 | 395.6 | 1782 | 457.1 | 46.70 | 15.85 | 43705 | 68.0 | | | | | | | | | | | 3.32 |
| 121/14-08-006-13W2 | 52 | 170 | 6.88 | 6.11 | 391.1 | 34.6 | 35000 | 451.8 | 1388 | 474.5 | 62.02 | 27.19 | 47200 | 73.5 | | | | | | | | | | | 4.02 |
| 121/14-13-006-14W2 | 52 | 112.5 | 6.62 | 6.27 | 422.0 | 52.8 | 27040 | 294.4 | 1399 | 378.1 | 53.06 | 19.57 | 39440 | 61.0 | | | | | | | | | | | 4.16 |
| 141/08-07-006-13W2 | 58 | 165 | 6.57 | 6.01 | 358.8 | 123.6 | 27730 | 337.3 | 1559 | 390.8 | 84.07 | 22.08 | 42315 | 74.5 | | | | | | | | | | | 3.95 |
| 141/08-12-006-14W2 | 56 | 210 | 6.79 | 6.35 | 386.9 | 49.3 | 29550 | 584.1 | 1615 | 371.1 | 39.39 | 19.75 | 46375 | 72.5 | | | | | | | | | | | 4.22 |
| 141/08-23-006-14W2 | 58 | 155 | 7.00 | 6.55 | 470.7 | 188.6 | 24750 | 404.0 | 1359 | 361.5 | 39.11 | 25.65 | 36880 | 52.0 | | | | | | | | | | | 2.48 |
| 141/14-06-006-13W2 | 56 | 100 | 6.84 | 6.42 | 710.5 | 17.2 | 29730 | 322.7 | 1373 | 425.8 | 31.76 | 29.35 | 51800 | 96.5 | | | | | | | | | | | 3.98 |
| 141/14-07-006-13W2 | 56 | 135 | 6.85 | 6.09 | 371.6 | 136.4 | 34990 | 746.1 | 1552 | 395.1 | 45.70 | 25.63 | 53400 | 80.0 | | | | | | | | | | | 4.64 |
| 141/14-11-006-14W2 | 53 | 115 | 6.50 | 5.9 | 389.3 | 103.5 | 29200 | 512.7 | 1760 | 387.0 | 35.64 | 22.91 | 45000 | 71.0 | | | | | | | | | | | 9.69 |
| 141/14-18-006-13W2 | 55 | 210 | 6.31 | 6.05 | 437.1 | 182.9 | 19920 | 393.0 | 1238 | 363.8 | 79.68 | 25.59 | 32875 | 56.5 | | | | | | | | | | | 5.25 |

424

425

426

427

428

429

430

431

432

433

434

435

436

437

438

Srivastava and Huang (1997) and Srivastava et al. (2000) report CO₂ solubility in oil, and oil gravity, an important control on the solubility of CO₂ (Mungan, 1981). API Gravity in the Weyburn field varies from 25°-38° (Srivastava et al., 2000). CO₂ solubility is reported for three wells, W1 (14-17-6-13 W2), W2 (3-11-7-13 W2) and W3 (12-18-6-13 W2 horizontal) in the Phase 1A area. Srivastava et al. (2000) report the initial solubility of CO₂ for their wells W1 and W2 as 70 sm³/m³ (standard cubic meters per cubic meter) and 40 sm³/m³ for well W3 (see Figure 1 for well locations). Note that these solubilities, derived from Srivastava et al. (2000) correspond to pCO₂ of 70 bar, well in excess of the maximum pCO₂ of 18.1 bar observed for the Phase 1A baseline samples. At the initial pre injection conditions of pCO₂ for the low TDS (pCO₂ = 6.3 bar) and high TDS (pCO₂ = 1.3 bar) wells, data from Srivastava et al. (2000) suggest the CO₂ content of the oil is close to 0.0. At the end of injection model conditions of 60°C and 170 bar, the solubility of CO₂ in oil calculated from Srivastava et al. (2000) is 560 sm³/m³ for W1, 640 sm³/m³ for W2 and 330 sm³/m³ for W3. A similar calculation using the ending pCO₂ after 50 years of injection and solubility in oil gives the ending amount of CO₂ stored in oil. The

difference between starting and ending amounts represents additional CO₂ storage per unit volume of oil at the end of injection.

5. Estimating CO₂ Storage Budgets in the Weyburn Reservoir

There are four main ways in which injected CO₂ can be stored in the Weyburn oil field:

1. In saline formation water as dissolved species
2. As minerals, primarily carbonates, including dawsonite
3. In oil, as a dissolved species
4. As supercritical CO₂

We combined the analytical data reported in section 4 with geochemical modeling to assess which mechanisms contribute to storage of injected CO₂ in the Weyburn reservoir, and to what extent.

Although the Weyburn reservoir is dominantly calcite, dolomite and anhydrite, significant concentrations (1-5 wt%) of potentially reactive silicate minerals are present and may assist in CO₂ storage. Reaction of CO₂-charged fluid with silicate mineral assemblages may allow trapping of additional CO₂, especially if reservoir containment is compromised, because CO₂ can be trapped as carbonate minerals. Equilibrium models are examined first to determine the sensitivity of CO₂ storage to variations in mineralogy and fluid composition, to suggest potential reacting phases for kinetic models, and to provide a starting point for kinetic models. Kinetic models are then examined to approximate the timing of various reactions and to contrast with equilibrium models employed in the Wilson and Monea (2004) estimates of mineral storage (45.14 MT). Various poorly known parameters, including mineral surface areas and dissolution and precipitation rates, can have a significant effect on estimated reaction times. However, the relative timing of reactions at least qualitatively indicates the reactions that dominate at various stages of CO₂ storage. One published model of the Weyburn project indicates that dawsonite forms within a year (Cantucci et al., 2009) and also suggests that K-feldspar dissolves and subsequently precipitates, along with muscovite and albite, within the first 14 years. They note that in their simulations after 100 years, the silicates have not achieved equilibrium.

5.1 Geochemical Simulations of Mineral-Saline water-CO₂ Interaction

The objective of equilibrium geochemical simulations is to show the relative impact of water composition and potential reactions that may dissolve or precipitate different mineral phases,

not to provide a timeline or to quantify storage. Previous estimates of mineral storage at Weyburn (Wilson and Monea, 2004) using equilibrium models probably greatly overestimate actual mineral storage of injected CO₂. The amount of additional CO₂ stored as minerals and dissolved in saline formation water is therefore first modeled as though a slug of CO₂ is added stepwise and reacts with the water and minerals, either first as an equilibrium and subsequently as a kinetic model. The difference between the baseline amount of CO₂ in the saline water and the final amount produced as minerals, as ionic species, and as dissolved CO₂ is considered to be additional stored CO₂. During this stage of modeling, which covers the injection period (50 years), pure supercritical CO₂ is available to the mineral-saline water system.

At Weyburn the temperature and pressure are variable, but an average of 170 bars (1700 KPa) and 60°C is representative. The initial state of the rock-water system was set by equilibrating minerals (Muscovite:Al, Dolomite:Mg, K-feldspar:K, Calcite:pH, Anhydrite:SO₄, Albite:SiO₂) with water representative of baseline conditions as outlined previously.

Table 3. Rate Constants and Modelling Parameters

| "Acid" rate | | n1 | Specific Surf Area (m²/g) | | Reference |
|--------------------|------------------------------------|-----------|---|--------------|-------------------------|
| Mineral | log k (mol/m²•s) | | Marly | Vuggy | |
| K-feldspar | -10.06 | 0.5 | 0.175 | 0.175 | Palandri & Kharaka |
| Calcite | -0.3 | | 0.034 | 0.015 | Palandri & Kharaka |
| Dol-dis | -3.19 | 0.5 | 0.105 | 0.014 | Palandri & Kharaka |
| Kaolinite | -11.31 | 0.777 | 2.317 | 0.015 | Palandri & Kharaka |
| Montmorillonite | -12.71 | | | | Palandri & Kharaka |
| Smectite | -10.98 | | | | Palandri & Kharaka |
| Albite | -10.16 | 0.457 | | | Palandri & Kharaka |
| Anhydrite | -3.19 | | 0.1 | 0.1 | Cantucci |
| Dawsonite | | 0.982 | 0.14 | 0.14 | Hellevang et al. (2010) |
| Quartz | -13.4 | | | | Palandri & Kharaka |
| Am Silica | -12.23 | | | | Palandri & Kharaka |

| Neutral Rate | | Specific Surf Area (m²/g) | | Reference |
|---------------------|------------------------------------|---|--------------|-------------------------|
| Mineral | log k (mol/m²•s) | Marly | Vuggy | |
| K-feldspar | -12.41 | 0.175 | 0.175 | Palandri & Kharaka |
| Calcite | | 0.034 | 0.015 | Palandri & Kharaka |
| Dol-dis | -3.19 | 0.105 | 0.014 | Palandri & Kharaka |
| Kaolinite | -13.18 | 2.317 | 0.015 | Palandri & Kharaka |
| Montmorillonite | -14.41 | | | Palandri & Kharaka |
| Smectite | -12.78 | | | Palandri & Kharaka |
| Albite | -12.56 | | | Palandri & Kharaka |
| Dawsonite | | 0.14 | 0.14 | Hellevang et al. (2010) |
| Quartz | -13.40 | | | Palandri & Kharaka |
| Am Silica | -12.23 | | | Palandri & Kharaka |

487

488 Kinetic and equilibrium reaction path models were set up according to the mineralogy based on

489 the average of the LPNORM mineral modes for Vuggy and Marly flow units. The solubility of

CO₂ was calculated (Duan and Sun, 2003) to be 0.985 mol/Kg (low TDS) at 60°C, 170 bar and 0.83 M NaCl and 0.841 mol/Kg (high TDS) at 1.67 M NaCl. In the simulations, CO₂ is added in a reaction path calculation until the calculated solubility of CO₂ is reached. This represents the point at which CO₂ no longer will dissolve in the aqueous phase and further addition of CO₂ must be present in a separate gas or supercritical phase. Plagioclase, K-feldspar and Illite (as muscovite), included in the reaction path calculation, are present in the samples. The amount of CO₂ required to reach the solubility value includes CO₂ dissolved in saline water and CO₂ stored in minerals. Examination of LPNORM results shows that plagioclase is either 100% albite component, or is dominated by albite (Na plagioclase), therefore no anorthite (Ca component) is initially present in the simulation, limiting the formation of calcite due to reaction of anorthite. However, dawsonite (NaAlCO₃(OH)₂) could potentially form, either from dissolution of albite, or from reaction with Na⁺ derived from the saline formation water. The water-rock ratio is required for reaction path models and was determined using LPNORM mineral amounts for each flow unit, the density of the high and low TDS formation water, and the fraction of the porosity that is water saturated.

5.1.1 Equilibrium Reaction Model

Representative equilibrium reaction path results for the Marly (M0) are shown in **Figure 4**. Results for the Vuggy flow units are similar in terms of the reactions, although amounts of minerals formed and dissolved are different. In the simulations, aluminous silicates are present in all samples in small amounts (1-5 wt %) and are consumed rapidly as CO₂ is added. Calcite and dolomite amounts are little affected and a small amount of anhydrite is dissolved, reflected by an increase in sulfate concentrations in saline water. A small amount of calcite is precipitated due to the Ca²⁺ produced by dissolution of anhydrite. K-feldspar is dissolved throughout the reaction path, producing muscovite (proxy for illite). Compositions of produced water, discussed later, suggest that chalcedony is the likely silica polymorph, rather than quartz. Dawsonite (Na-Al carbonate) is produced initially from Na⁺ and Al³⁺ derived from albite dissolution and, once albite is consumed, from Na⁺ in the saline water. The pH decreases from 6.6 to 4.7 over the course of the simulation. The main limiting factor for consumption of CO₂ due to mineral reactions is the amount of dawsonite that forms, which in turn is limited by the amount of Na⁺ and Al³⁺ available, either in the saline formation water or by dissolution of albite. The dissolution of albite is limited by the kinetics, and the rate of this process is considered in the next section. Equilibrium is unlikely to be reached within decades, therefore to evaluate the time frame of CO₂

storage, reaction rates (kinetic simulations) are addressed after the equilibrium condition is considered.

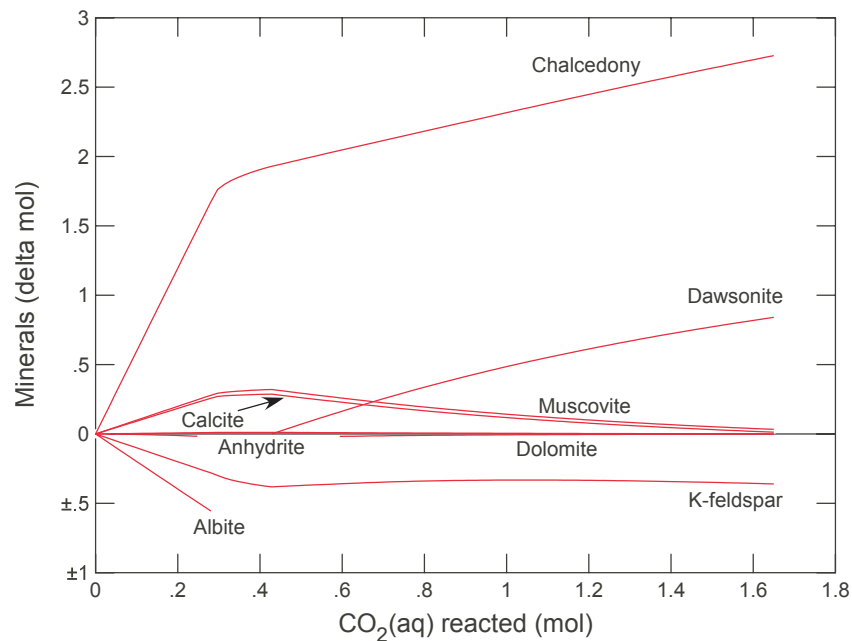


Figure 4. Equilibrium reaction path simulation of addition of CO₂ to M0 flow unit at 60°C and 1 bar.

5.1.2 Kinetic Reaction Model

The kinetic reaction model is based on the equation:

$$r = A_s k_+ \left(1 - \frac{Q}{K}\right)$$

where r is the reaction rate, A_s is the mineral surface area, k_+ is the dissolution rate constant, Q is the activity product and K is the equilibrium constant for the dissolution reaction. This rate law is based on transition state theory (Lasaga, 1984). The temperature dependence of the rate constant is based on the Arrhenius equation (Lasaga, 1984; Steefel and Lasaga, 1994).

Shevalier et al. (2013) showed that over a ten-year period at Weyburn, calcite saturation index calculations for produced water show calcite to be near equilibrium, although due to large variations in CO₂ injection volumes and rates, the variations in saturation states are large. Dolomite dissolution is expected from the models presented here, therefore the precipitation of dolomite, which is known to be slow, was not considered. Mineral surface areas strongly

influence overall reaction rates. For silicate minerals in the Marly and Vuggy core samples, the surface area was calculated from the average observed grain size in SEM and TS and using the surface area (A) formulae for either a prism ($A = 2ab + 2bc + 2ac$) or a cube ($A = 6a^2$) as appropriate from the mineral morphology. The surface areas, and therefore the reaction rates, are certainly overestimates as the entire surface is not available to react with fluids. As the minerals present dissolve or precipitate, surface area changes and these changes are calculated within REACT. Further, experiments by Yang et al. (2008) for Weyburn saline water suggest the CO₂ saturated formation water has intermediate wettability. In other words the surface of the rock is likely to be partly oil-wet, further reducing the mineral surface area available for reaction and decreasing the overall extent of reaction.

The rate data for dawsonite suggest that it should form rapidly (within years). However Hellevang et al. (2011, 2013) suggest that dawsonite, in spite of being present in theoretical calculations, may not form, or may not persist. Dissolution rates for dawsonite are from Hellevang et al., (2010), and the rates presented there are more rapid than those reported in Hellevang et al. (2005) and Palandri and Kharaka (2004). At Weyburn, plagioclase is dominated by the Na component, albite and, based on the natural analogues described in the introduction, it is feasible that dawsonite may precipitate as albite is dissolved.

Figure 5 shows typical results of a kinetic simulation for the M0 flow unit and high TDS water. The parameters used in the simulations are shown in Table 3. The results, in terms of CO₂ amounts in various phases, are presented in a later section. Due to the very slow dissolution rate of albite, which provides the essential constituents to form dawsonite (Na⁺ and Al³⁺), the differences in amounts of albite have limited impact on the total storage of CO₂. As reaction rates and surface areas for the minerals involved are not well known, the surface areas and reaction rates were increased by an order of magnitude, but this causes little or no change in the amount of reaction and thus the amount of CO₂ required to reach saturation in the saline formation water. Figure 5 shows precipitating minerals as positive amounts and dissolving minerals as negative amounts. Initially, muscovite (proxy for illite) dissolves, precipitating K-feldspar. The simulations show that 31 cm³ of dawsonite, per Kg of water, forms at the end of 50 years. Chalcedony and kaolinite also precipitate, in amounts less than 5 cm³ over the entire simulation. To place the amounts of minerals in perspective, for 1 Kg of water at the porosity of the M0 flow unit, there is 9813 cm³ of rock. The 31 cm³ of dawsonite formed is miniscule in this context, and were post-CO₂ injection core examined after 50 years, the amounts of minerals

precipitated and dissolved would likely be undetectable, especially in the context of the observed natural variations in mineral amounts.

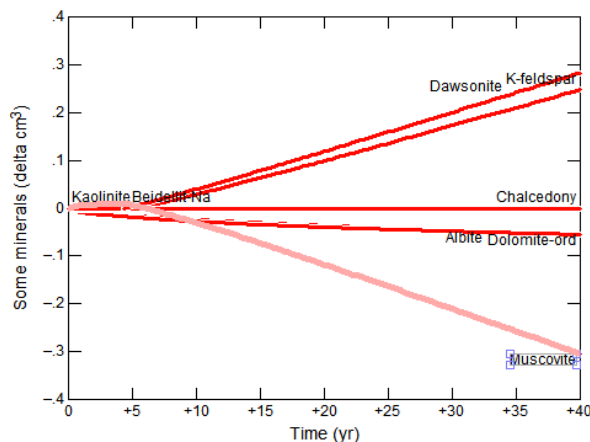


Figure 5. Kinetic reaction path simulation of addition of CO₂ to M0 flow unit at 60°C and 1 bar.

As expected, storage of CO₂ in minerals is considerably different between equilibrium and kinetic models. Figure 6 shows the amount of CO₂ stored by mineral reactions per Kg of water, in each flow unit. Equilibrium models show storage ranging from 0.4 to 2.7 mol CO₂ per Kg of water. Kinetic models all show storage of less than 0.2 mol CO₂ per Kg of water, and as low as 0.01 mol CO₂ per Kg of water. The equilibrium models show a strong dependence of CO₂ storage on flow unit mineralogy. For kinetic models, mineralogical differences have a much lesser, but still detectable effect over the 50-year injection period. Differences in CO₂ storage due to mineral reactions for either equilibrium or kinetic simulations primarily reflect dissolution of greater amounts of muscovite and albite to form dawsonite. Generally, the presence of high TDS formation water results in formation of more dawsonite, due to the higher Na⁺ content of the saline water, and the resulting storage of more CO₂. More CO₂ is stored in the low TDS formation water due to greater solubility. Overall, it is clear that the mineral storage amounts (22.25 MT) published by Wilson and Monea (2004) based on equilibrium modeling greatly overestimate mineral storage at Weyburn.

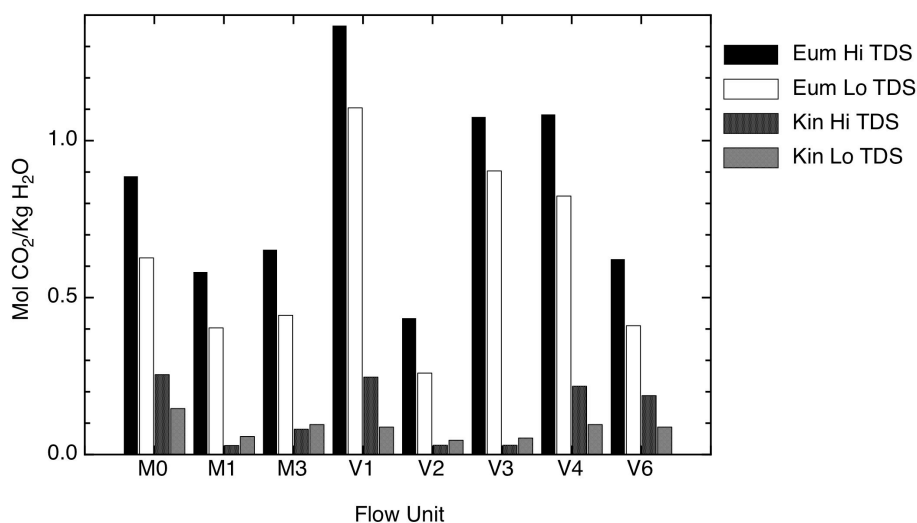


Figure 6. Mineral storage of CO₂ by flow unit for equilibrium and kinetic models. “Eum” refers to equilibrium models, “Kin” refers to kinetic models “Hi” is high, and “Lo” is low.

Once injection stops, no more CO₂ is added. The silicates have not come to equilibrium at the end of injection (50 years), and will continue to react with the CO₂ remaining in the supercritical CO₂ fluid, the saline formation water and the oil. During this stage of modeling, pure supercritical CO₂ is no longer being added and the CO₂ present will eventually be consumed by reaction with saline water and minerals. Although reaction that continues after injection stops will not change the amount of CO₂ that can be stored, it will redistribute the CO₂ in the system. At the end of injection CO₂ is present as a supercritical phase and dissolved in oil and saline water. As the reservoir “soaks” when injection stops, an increasing amount of CO₂ is trapped in minerals. Accordingly, one simulation (Figure 8, M0, high TDS) was completed for 5000 years, with the fugacity of CO₂, the saline water composition, and the amounts of reactive minerals initially set to the values at the end of the 50-year injection period. Assuming the pressure and temperature at the end of injection are similar to the start of injection, the fCO₂ at 170 bars and 60°C, calculated from Duan and Sun (2003) is 85 bars. At the start of the 5000-year simulation, per Kg of fluid, there is 116 cm³ of anhydrite, 2285 cm³ of calcite, 30 cm³ of dawsonite, and 5831 cm³ of dolomite. After 5000 years, there is 107 cm³ of anhydrite, 2302 cm³ of calcite, 87 cm³ of dawsonite, and 5832 cm³ of dolomite. Total mineral volume per Kg of water has increased from 8262 to 8324 cm³. As Figure 7 shows, over the 5000 years, the fugacity of CO₂ has decreased from 85 bar to 1 bar. Total carbon in the fluid initially is 1.47 mol/Kg and at the end it is 0.04 mol/Kg, the difference being transferred from the saline formation water, supercritical fluid and oil, to the minerals.

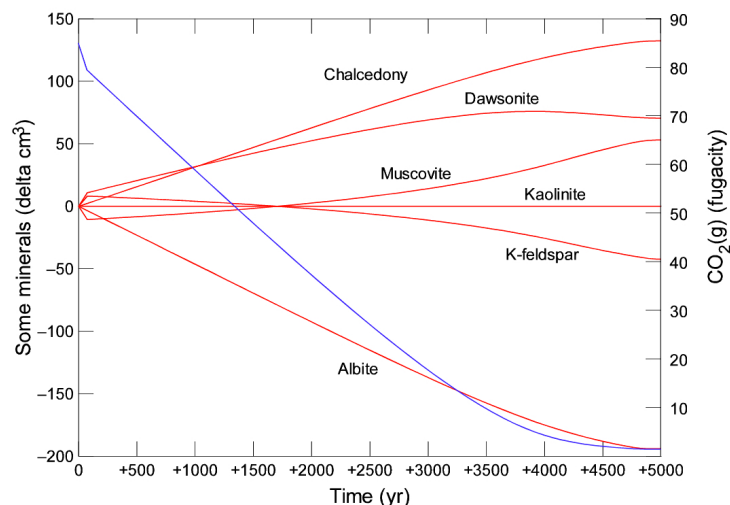
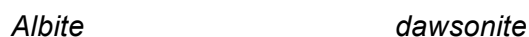
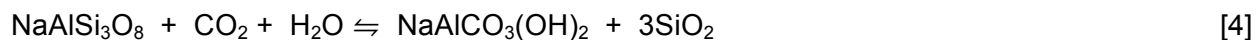
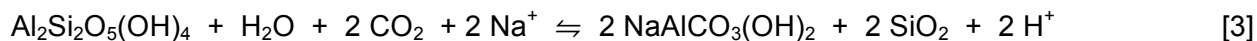


Figure 7. Kinetic simulation of M0 flow unit for high TDS saline formation water at 60°C and starting $f\text{CO}_2 = 85$ bar, showing the evolution of mineral amounts at the end of injection over 5000 years. Red lines represent the difference in mineral amounts. The blue line is the change in CO_2 fugacity. Note that time 0 is after 50 years of CO_2 injection and no additional CO_2 is added during the simulation.

5.2 Dawsonite Formation

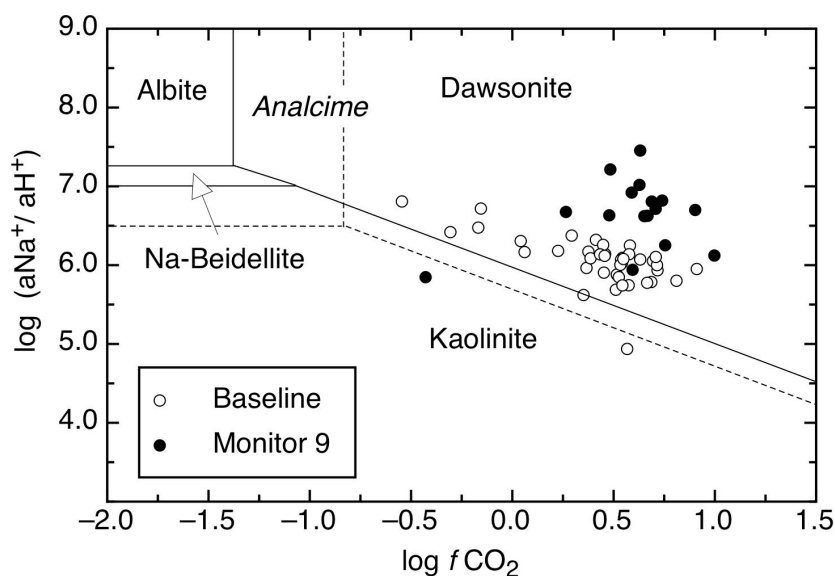
Analyses of formation waters from the Weyburn reservoir can be compared to the stability of dawsonite, relative to kaolinite, albite and Na-beidellite, a component in smectite. Hellevang et al. (2005, 2010, 2011 and 2013) suggest that there are significant barriers to dawsonite formation. It is not possible to prove with the existing data that dawsonite has formed at Weyburn as a result of CO_2 injection, but produced water and gas analyses are available to examine the state of produced waters relative to dawsonite stability. The relevant reactions are:



In addition to temperature and pressure, the relevant variables are the fugacity of CO_2 ($f\text{CO}_2$), the activity ratio of Na^+/H^+ , and the activity of aqueous SiO_2 . Two equilibrium phase diagrams, similar to those presented by Hellevang et al. (2011) calculated using ACT2 (Geochemists Work

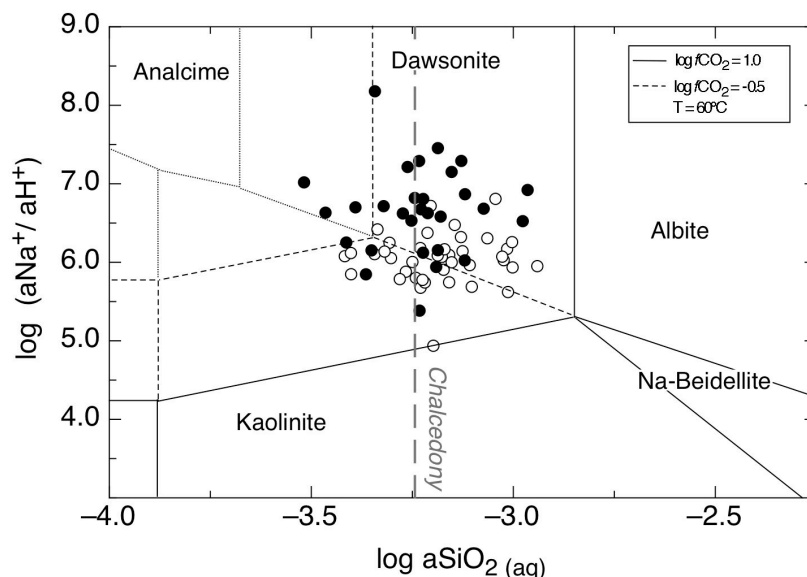
646 Bench®) portray the stability of dawsonite relative to kaolinite, albite and Na-beidellite.
 647 Hellevang et al. (2013) suggest that analcime may form from albite dissolution rather than
 648 dawsonite. Figure 8a shows $\log f\text{CO}_2$ versus the log of the activity ratio of Na^+/H^+ , Figure 8b
 649 shows a $\text{SiO}_2(\text{aq})$ versus the log of the activity ratio of Na^+/H^+ .

650



651

652



653

654 Figure 8. The stability of dawsonite at 60°C and 1 bar. (a) The activity of aqueous SiO_2 is set by
 655 equilibrium with chalcedony. Solid boundaries represent stability of dawsonite relative to albite.
 656 Dashed boundaries represent stability relative to analcime. (b) Dotted lines show analcime
 657 stability with dawsonite suppressed. Dashed ($\log f\text{CO}_2 = -0.5$) boundaries and solid boundaries

(log $f\text{CO}_2 = 1.0$) show the stability of dawsonite relative to albite, kaolinite and Na-beidellite (smectite). The range of log $f\text{CO}_2$ at Weyburn is between -0.5 and 1.0.

Plotted on the phase diagrams (Figure 8a, b) are baseline formation water compositions (open circles) and produced water compositions from Monitor 9 (M9, 3 years after start of injection, closed circles). Baseline fluid compositions are from Emberley et al. (2005), M9 fluid compositions are shown in Table 2. The activity of the requisite species was calculated using SOLMIN88 (Kharaka et al., 1988) by the methods outlined in Shevalier et al. (2013) to determine the pH and species activity at reservoir conditions. Figure 8b shows that the water compositions tend to cluster around saturation with respect to chalcedony. Fluid compositions from Baseline to M9 trend towards increasing stability of dawsonite, primarily due to decrease in pH between baseline and M9 (Shevalier et al., 2013). Mineral species that exist as solid solutions will have lower activities of the thermodynamic component (e.g., the Na-feldspar albite as a component in plagioclase), and this will cause the stability fields to enlarge. However, at Weyburn the plagioclase is observed to be primarily albite component, and the other minerals (kaolinite, analcime and dawsonite) show little or no solid substitution, therefore the stability fields are unaffected. An exception is Na-beidellite, a component of smectite. If smectite were to form during CO_2 injection, the activity of Na-beidellite (the Na component in the mineral smectite) would likely be less than one, and this could cause a significant increase in the stability field, potentially causing Na-beidellite to encompass the observed fluid composition range to the exclusion of dawsonite and analcime. No post- CO_2 core was available from Weyburn, so the possible existence of dawsonite or smectite (beidellite) as a product of CO_2 injection is not known. Modeling by Abercrombie et al. (1994) suggests that silica activities, that range from -3.5 to -3.0 by Monitor 9 (Figure 8), are within the range necessary to precipitate smectite. Our modeling also shows that other zeolite minerals, including mordenite and clinoptilolite, are more stable than dawsonite and need to be suppressed to present the stability field of dawsonite. It is not known if any zeolite minerals have formed as a result of CO_2 injection at Weyburn, so the relative stability of these zeolites was not pursued.

The composition of produced fluids suggests that water compositions resulting from injection of CO_2 are within the stability field of dawsonite and that injection of CO_2 favours increased stability of dawsonite. Figure 5 shows a kinetic reaction path simulation showing dawsonite may begin to precipitate as muscovite (source of aluminum) dissolves and this may occur within 5-10 years of commencement of CO_2 injection. However, these observations do not require that

dawsonite actually forms or persists. Nucleation difficulties and the availability of sufficient Al^{3+} in solution could prevent or attenuate dawsonite precipitation (Hellevang et al., 2013). Further, at Weyburn the dissolution of potential silicate precursors (albite, kaolinite and K-feldspar) is probably overestimated as they occur in small amounts (0.3-9 wt%) and are not totally exposed to the injected fluids. Further, the dissolution of silicate precursors and the precipitation of dawsonite could be inhibited by the presence of oil in the porosity. In the absence of examination of post-injection core it is not possible to determine whether or not dawsonite has formed in the Weyburn reservoir.

6. Storage of CO_2 in Minerals, Gas, Oil and Saline water

To estimate potential storage of CO_2 at Weyburn requires estimates of the pre-injection amount of CO_2 in each phase (oil, gas, saline water, minerals) and the final amounts in those phases. Geochemical simulations, combined with the pore volume saturated with saline water, allow an estimate of CO_2 stored in saline formation water and minerals during 50 years of injection at Weyburn. White et al. (2004) give starting oil saturation as 0.53 in the Marly and 0.35 in the Vuggy. Because only saline formation water and oil (at the start of injection there is no free gas phase present) are present prior to CO_2 injection, saline water saturations are 0.47 in the Marly and 0.65 in the Vuggy. However, at the end of injection, CO_2 also will be resident in unrecoverable oil (irreducible oil) and in a remaining supercritical CO_2 -rich fluid phase. The additional information required to estimate CO_2 storage in the Phase 1A area at Weyburn includes:

1. The total pore volume of each flow unit.
2. The starting and ending saturation of that pore volume with oil, saline water and CO_2 supercritical fluid.
3. The initial and final amount of CO_2 in oil.
4. The starting and ending amount and composition of the CO_2 supercritical fluid phase.

Table 4 shows the pore volume of major units at Weyburn (Geoff Burrowes and Stan Wright, Cenovus, personal communication). In the Phase 1A area the Marly has a pore volume of approximately $34 \cdot 10^6 \text{ m}^3$ and the Vuggy has a pore volume of approximately $40 \cdot 10^6 \text{ m}^3$. Within the Marly the greatest pore volume is in the M3 flow unit ($16.8 \cdot 10^6 \text{ m}^3$) and in the Vuggy the greatest pore volume is in the V2 ($15.4 \cdot 10^6 \text{ m}^3$) flow unit. The relative volume fraction saturations at the end of CO_2 injection with respect to oil-water-gas for the Marly are projected

725 to be 0.3/0.5/0.2 and 0.2/0.7/0.1 for the Vuggy (Geoff Burrowes and Stan Wright, Cenovus,
726 personal communication).
727

Table 4. Pore Volume (m³) of Flow Units, Weyburn Phase 1A Area.

| Flow Unit | Volume (m³) |
|------------------------|-------------------------------|
| Marly (All flow units) | 3.40E+07 |
| Vuggy (All flow units) | 3.99E+07 |
| Marly M0 | 5.31E+06 |
| Marly M1 | 9.54E+06 |
| Marly M2 | 2.37E+06 |
| Marly M3 | 1.68E+07 |
| Vuggy V1 | 6.90E+06 |
| Vuggy V2 | 1.54E+07 |
| Vuggy V3 | 1.99E+06 |
| Vuggy V4 | 4.27E+06 |
| Vuggy V5 | 4.61E+06 |
| Vuggy V6 | 6.72E+06 |

728

729 The amount of CO₂ stored as minerals and saline formation water is estimated from the reaction
730 path simulations. For the estimates presented below, only the kinetic results are used. It is

assumed that at the end of injection, the supercritical fluid is 100% CO₂. From the fluid-saturated pore volume, the molar amount of CO₂ stored in supercritical fluid CO₂ can be calculated from the specific volume of CO₂ (65.75 cm³/mol at 60°C and 170 bar: Duan et al, 1992).

The way in which injected supercritical CO₂ behaves with respect to the reservoir geometry, and dissolution in oil and saline formation water is complex. Detailed reservoir modeling, not attempted here, is required to determine distribution of CO₂ (and other gas species) during the injection period. To obtain an estimate of the amount of CO₂ in saline water, oil and as a gas or supercritical phase, we consider only the initial (pre injection) and final (end of injection) state. The injection of supercritical CO₂ may bypass the oil zones due to buoyancy override and arrive directly at production wells. During Weyburn oil field operations, CO₂ at producing wells is captured and re-cycled into injection wells. A zone of supercritical CO₂ may be present within the upper part of the reservoir units at Weyburn, but the extent of such a phase, if present, is unknown. However, a significant fraction of the injected supercritical CO₂ dissolves in the oil, as evidenced by the data of You et al. (2013). At Weyburn in the Phase 1A area there was no free gas phase present before CO₂ injection, therefore no CO₂ (or any other species) is present as gas initially at the reservoir level. However, prior to CO₂ injection, pressure drop during production causes CO₂, H₂S, CH₄ and higher carbon number (at least up to C₅) gas species that initially are dissolved in oil and saline water, to be produced at surface. After injection started in September of 2000, the fraction of CO₂ produced as a gas at surface, increased with time (Mayer et al., 2013). Continued injection of CO₂ is expected to eventually produce either a gas or supercritical CO₂-rich fluid phase at the reservoir level and once this has formed, it is expected that the CO₂, H₂S, CH₄ and higher carbon number gas species will be distributed between the saline formation water, oil and a gas/supercritical fluid phase.

The calculation for CO₂ solubility in oil assumes that CO₂ comes rapidly (within years) to solubility equilibrium with the oil. Only the starting (pre CO₂ injection) and final (end of CO₂ injection) amounts are considered, thus the amount of CO₂ in oil will be maximized. Pre injection concentrations of CO₂ in oil are less than 5 mol % (Srivastava et al., 2000). Results from You et al. (2013) show that after ten years, CO₂ content of the oils is as high as 38.5 mol percent, confirming that CO₂ is dissolving rapidly in the oil. The initial amount of CO₂ in oil is calculated from the results of Srivastava et al. (2000) and the pore volume fraction saturated with oil. The ending amount is calculated from the final oil saturated pore volume and the solubility of CO₂ in

oil as calculated according to procedures described in the Methods section. The difference between the initial CO₂ in oil and the final amount of CO₂ in oil at elevated pCO₂ represents additional CO₂ storage in oil. As previously noted, the greater buoyancy of a CO₂ rich supercritical phase might cause it to bypass some of the oil within the reservoir, reducing the total amount of CO₂ estimated to be captured in oil at Weyburn. Detailed reservoir modeling, incorporating flow and the distribution of gas, comprised of CO₂, H₂S and C₁-C₅₊ hydrocarbons, is required to estimate the degree of this effect. Such modeling is beyond the scope of this paper.

Combining the results of mineral, saline formation water, gas and oil calculations and the pore volume saturated with saline water, gas and oil at the end of injection, allows the total storage of CO₂ to be calculated for Phase 1A at Weyburn at the end of injection (here assumed to be 50 years). Figure 9 shows, by flow unit, the total tonnes of CO₂ in saline formation water (low and high TDS), minerals (low and high TDS), oil (W1 and W3, representing high and low solubility, respectively) and gas or supercritical fluid. The following numbers need to be placed in the context that between 2000 and 2012, 22 million tonnes of CO₂ have been injected over the entire Weyburn field (Petroleum Technology Research Centre, 2014), although this number is certainly greater at the time of writing and will increase until the end of the oil recovery project. Total storage of CO₂ in Phase 1A dissolved in oil is the largest sink, ranging from $6.5 \cdot 10^6$ to $1.3 \cdot 10^7$ tonnes, depending on solubility. Storage in the supercritical CO₂-rich phase, is significant, approximately $7.2 \cdot 10^6$ tonnes, and greater than in minerals (range from $2 \cdot 10^5$ to $6 \cdot 10^5$ tonnes) and saline formation water (range from $1.5 \cdot 10^6$ to $2 \cdot 10^6$ tonnes). Storage of CO₂ by solubility in the oil, even after the reservoir has been depleted near to irreducible oil saturation, is greater than storage in the supercritical CO₂ phase, in saline water and in minerals.

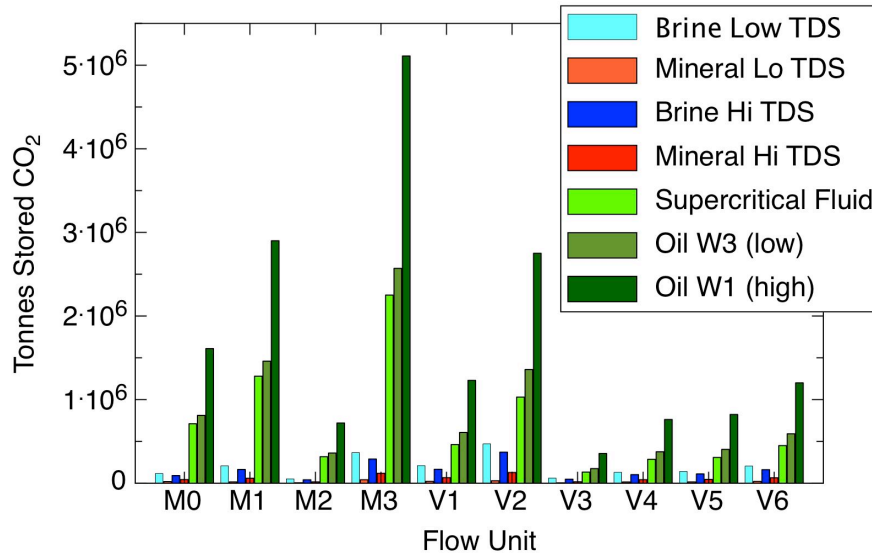


Figure 9. Storage of CO₂ in supercritical fluid, saline formation water, minerals and oil at the end of 50 years of injection at the Phase 1A area in Weyburn.

7. Discussion

By the calculations outlined above, oil at Weyburn Phase 1A represents potentially the largest sink for injected CO₂, even though oil represents by volume only 30% and 20% respectively, of the estimated final pore saturation of the Marly and Vuggy flow units. This is primarily due to the fact that at Weyburn the oil is high API gravity (low density), has relatively high CO₂ solubility and, prior to CO₂ injection, has a very low amount of dissolved CO₂. Also, prior to injection of CO₂ the oil has very low gas saturation, and there is no free gas phase in the reservoir. Further, the gas components initially dissolved in oil include H₂S and C₁-C₅₊ hydrocarbon gas, in addition to relatively low amounts of CO₂ (Emberley et al., 2005), therefore CO₂ initially represents a relatively small proportion of the gas species dissolved in oil. The very high CO₂ solubility of Weyburn oil, combined with the low amount of CO₂ in oil and saline water prior to CO₂ injection, results in significant calculated storage of CO₂ in oil at the end of injection. In addition, relatively short-term (50+ years) storage in oil at Weyburn is comparatively secure. At the end of injection of CO₂ and economic oil recovery, most of the oil is trapped in the pore volume by strong capillary forces. Only a catastrophic decrease in pressure would release the CO₂ from solution in the oil.

Various factors will affect the calculated versus the actual amounts of CO₂ stored at Weyburn over the 50-year injection period. The amount of solubility storage in oil is strongly dependent on the final oil saturations, which are unknown and will be variable across the Weyburn field. Further, the solubility data for CO₂ in oil are restricted to the northern part of the Weyburn field. Generally oil density (Figure 1) decreases (API gravity increases) over the rest of the Weyburn field, so storage in oil will probably be at least equal to the highest measured value, 640 sm³/m³, or greater. Finally, as noted previously, buoyancy override of supercritical CO₂ may cause oil saturated zones to be bypassed, causing the amount of CO₂ captured in oil to be less than calculated here. Regardless of the unknown effect of the variation of CO₂ solubility in Weyburn oil, and bypassing of oil zones, solution of CO₂ in oil will probably be the dominant form of storage at Weyburn at the end of CO₂ injection.

The mineral surface areas and reaction rates in our calculations are poorly known. In our calculations, precipitation rates are assumed to be the same as dissolution rates, but are probably slower. Effective mineral surface areas are probably smaller than those used in simulations, further reducing the rate of reaction. Further, the presence of oil possibly wetting mineral surfaces (Yang et al., 2008) will decrease surface areas even more, resulting in less mineral storage of injected CO₂. Thus, the mineral estimates for the injection period (50 years) probably represent maximum mineral storage. Further, redistribution of injected CO₂ from the oil, saline formation water, and supercritical fluid to the minerals requires approximately 5000 years in the calculations presented, but because the mineral reaction rates are probably slower than those used here, this probably is a minimum time estimate.

The calculations do not couple flow, reaction rates and the resulting storage. Such calculations were not attempted. Although reactive transport is an important consideration, the data gathering required to frame these calculations leaves this as a next step to refine the results presented here. An outline of proposed reactive transport modeling at Weyburn is given in Johnson et al. (2011). Cavanagh and Rostron (2013) used high-resolution capillary flow simulations of migration pathways and recognize that the large number of wells and high well density in the Weyburn field result in a major challenge for conventional flow modelling.

The results presented here are for the Phase 1A area of the IEA GHG Weyburn Monitoring and Storage Project. However, they can be extrapolated to the entire Weyburn field if we assume that the mineralogy of the various flow units is similar to that determined for the Phase 1A area.

The resulting potential storage for the entire field would increase to approximately $1.7 \cdot 10^8$ tonnes of injected CO_2 from $2.3 \cdot 10^7$ for only the Phase 1A area.

8. Conclusions

1. Over a 50-year injection period at Weyburn Phase 1A, CO_2 dissolved in oil is the dominant form of CO_2 storage ($6.5 \cdot 10^6$ to $1.3 \cdot 10^7$ tonnes), followed closely by storage as a supercritical CO_2 phase ($7.2 \cdot 10^6$ tonnes). Storage of injected CO_2 in saline formation water (range from $1.5 \cdot 10^6$ to $2 \cdot 10^6$ tonnes) and mineral storage (range from $2 \cdot 10^5$ to $6 \cdot 10^5$ tonnes) are the smallest sinks. No additional CO_2 will be stored other than that injected over the 50 year period.
2. Simulations show that CO_2 present as a supercritical fluid, saline water, and dissolved in oil at the end of injection is redistributed over a period of at least 5000 years into dawsonite. However, it is not possible to show conclusively that dawsonite has formed at Weyburn. Other Na-silicates including zeolites, and clay minerals may form, but were not included in estimates of CO_2 mineral storage.
3. Although the Vuggy and Marly flow units have variable mineralogy, the modeled reactions that take place due to addition of CO_2 are similar. Simulations that consider the mineralogy of individual flow units, and thereby the effect of variations in mineralogy on storage of CO_2 in oil, saline formation water, and minerals, represent a second order influence on CO_2 storage at Weyburn.
4. The availability of Na, either dissolved in saline water or available in minerals such as plagioclase (albite), is an important factor in long-term mineral storage of CO_2 , due to the probable formation of dawsonite. Increased TDS, and thereby the amount of Na available in saline water, will increase the amount of CO_2 potentially stored in Na-containing minerals. It is also expected that the amount of CO_2 stored in saline formation water will decrease as TDS increases, due to the decrease in solubility of CO_2 with increasing TDS.
5. Projects targeting abandoned oil reservoirs as possible storage sites for CO_2 should focus on sites that have no gas phase at reservoir level and an oil phase that has initially low CO_2 content, but very high CO_2 solubility. Typically, these conditions will be present in relatively shallow reservoirs with oils of high API gravity (low density). The capillary trapping forces at the end of oil recovery will result in oil being a relatively secure storage sink for injected CO_2 over the short term of 100's of years.

881 Over the longer term of thousands to tens of thousands of years, the CO₂ dissolved
882 in saline formation water, supercritical fluid, and oil will be redistributed into mineral
883 phases, if sufficient volumes of reactive minerals are present.

References

- Abercrombie, H.J., Hutcheon, I.E., Bloch, J.D. and de Caritat, P., 1994. Silica activity and the smectite-illite reaction. *Geology* 22, 539-542.
- Assayag, N., Matter, J., Ader, M., Goldberg, D and Agriner, P., 2009. Water–rock interactions during a CO₂ injection field test: Implications on host rock dissolution and alteration effects. *Chemical Geology* 265, 227-235.
- Baker, J.C., 1991. Diagenesis and reservoir quality of the Aldebaran Sandstone, Denison Trough, eastcentral Queensland, Australia. *Sedimentology* 38, 819-838.
- Baker, J.C., Guo, P.B., Hamilton, P.J., Golding, S.D., Keene, J.B., 1995. Continental-scale magmatic carbon dioxide seepage recorded by Dawsonite in the Bowen-Gunnedah-Sydney basin system, Eastern Australia. *Journal of Sedimentary Research* A65, 522-530.
- Burrowes, G., 2001. Investigating CO₂ Storage Potential of Carbonate Rocks during Tertiary Recovery from a Billion Barrel Oil field, Weyburn, Saskatchewan: Part 2 - Reservoir Geology (IEA Weyburn Monitoring and Storage Project) Saskatchewan Energy Mines Miscellaneous Report 2001-4, 64-72.
- Burrowes, G., Gilboy, C. 2000., Investigating Sequestration Potential of Carbonate Rocks During Tertiary Recovery from a Billion Barrel Oil Field, Weyburn, Saskatchewan: The Geoscience Framework. IEA Weyburn CO₂ Monitoring and Storage Project Report., 2000.
- Cantucci, B., Montegrossi, G., Vaselli, O., Tassi, F., Quattrocchi, F., Perkins, E., 2009. Geochemical modeling of CO₂ storage in deep reservoirs: The Weyburn Project (Canada) case study. *Chemical Geology* 265, 181-197.
- Cavanagh, A. and Rostron, B., 2013. High-resolution simulations of migration pathways and the related potential well risk at the IEAGHG Weyburn–Midale CO₂ storage project. *International Journal of Greenhouse Gas Control* 16S, S15-S24.
- de Caritat, P., Bloch, J., and Hutcheon, I., 1994. LPNORM: a linear programming normative analysis code. *Computers and Geoscience* 20, 313-347.
- Duan, Z., Sun, R., 2003. An improved model calculating CO₂ solubility in pure water and aqueous NaCl solutions from 273 to 533 K and from 0 to 2000 bar. *Chemical Geology* 193, 257-271.
- Duan, Z.H., Moller, N., and Weare, J.H., 1992. An equation of state (EOS) for CH₄-CO₂-H₂O I: pure systems from 0 to 1000 C and from 0 to 8000 bar. *Geochimica et Cosmochimica Acta* 56, 2605-2617.
- Dunham, R.J., 1962. Classification of carbonate rocks according to depositional textures. In *Classification of Carbonate Rocks*, edited by W.E. Ham, 08-121. American Association of Petroleum Geologists Memoir 1.
- Durocher, K., Hutcheon, I., Shevalier, M., Mayer, B., Gunter, B., Perkins, E., Bloch, J., 2003. *Subtask 3.1: Reservoir (Baseline) Mineralogy Final Report*. IEA Weyburn CO₂ Monitoring and Storage Project, Regina: Petroleum Technology Research Centre.
- Durocher, K.E., Bloch, J., Perkins, E., Hutcheon, I., Shevalier, M., Mayer, B. and Gunter, W.D., 2005. Mineralogical Characterization of the Weyburn Reservoir, Saskatchewan, Canada: are mineral reactions driving injected CO₂ storage? Edited by M., Morris, T., Gale, J. and Thambimuthu, K. Wilson. *Proceedings of the 7th International Conference on Greenhouse Gas Control Technologies*. Oxford: Elsevier 2097-2101.
- Emberley, S., Hutcheon, I., Shevalier, M., Durocher, K., Mayer, B., Günter, W.D., Perkins, E.H., 2005. Monitoring of fluid-rock interaction and CO₂ storage through produced fluid

- sampling at the Weyburn CO₂-injection enhanced oil recovery site, Saskatchewan, Canada. *Applied Geochemistry* 20, 1131-1157.
- Ferrini, V., Martarelli, L., De Vito, C., Cina, A and Deda, T., 2003. The Koman dawsonite and realgar-orpiment deposit, northern Albania; inferences on processes of formation. *The Canadian Mineralogist* 41, 413-427.
- Gunter, W.G., Perkins, E.H., Hutcheon, I., 2000. Aquifer disposal of acid gases: modeling of water-rock reactions for trapping of acid waters. *Applied Geochemistry* 15, 1086-1096.
- Gunter, W.G., Bachu, S., Benson, S., 2004. The role of hydrogeological and geochemical trapping in sedimentary basins for secure geological storage of carbon dioxide. *Geological Society of London, Special Publication* 233, 129-145.
- Hellevang, H., Aagaard, P., Oelekers, P., Kvamme, B., 2005. Can dawsonite permanently trap CO₂? *Environmental Science and Technology* 39, 8281-8287.
- Hellevang H, Declercq J, Kvamme B and Aagaard P., 2010. The dissolution rate of dawsonite at pH 0.9 to 5 and temperatures of 22, 60 and 77 °C. *Applied Geochemistry* 25, 1575-1586.
- Hellevang, H., Declercq, J., Aagaard, P., 2011. Why is Dawsonite Absent in CO₂ Charged Reservoirs? *Oil & Gas Science and Technology* 66, 119-135.
- Hellevang, H., Aagaard, P., and Jahren, J., 2013. Will dawsonite form during CO₂ storage? *Greenhouse Gas Science and Technology* 4, 191-199.
- Hitchon, B., 2012. Best Practices for Validating CO₂ Geological Storage: Observations and Guidance From the IEAGHG Weyburn Midale CO₂ Monitoring and Storage Project. Edited by Brian Hitchon. Sherwood Park, Alberta: Geoscience Publishing. 353 p.
- Holm, L.W. and Josendal, V.A., 1974. Mechanism of oil displacement by carbon dioxide. *Journal of Petroleum Technology (Transaction AIME)* 257, 1427-1438.
- Holm, L.W., 1959. Carbon dioxide solvent flooding for increased oil recovery processes. *Petroleum Transactions* 216, 225-231.
- Hovorka, S., Benson, S., Doughty, C., Freifeld, B.M., Sakurai, S., Daley, T., Kharaka, Y., Holtz, M., Trautz, R.C., Seay Nance, H., Myer, L.R., and Knauss, K.G., 2006. Measuring permanence of CO₂ storage in saline formations: the Frio experiment. *Environmental Geosciences* 13, 105-121.
- Hutcheon, I., Shevalier, M., and Abercrombie, H.J., 1993. pH buffering by metastable mineral-fluid equilibria and evolution of carbon dioxide fugacity during burial diagenesis. *Geochimica et Cosmochimica Acta* 57, 1017-1027.
- IPCC (Intergovernmental Panel on Climate Change). *Prepared by Working Group III of the Intergovernmental Panel on Climate Change*. Edited by B., Davidson, O., de Coninck, H.C., Loos, M., Mayer, L.A. (Eds.) In: Metz. Cambridge, United Kingdom/New York, NY, USA.: Cambridge University Press, 2005.
- Jensen, G.K.S., Nickel, E.H., and Rostron, B.J., 2013. Refinement of the Weyburn-Midale geological and hydrogeological model: Developing a better framework to determine reservoir response to injected CO₂ and subsequent CO₂ movement. *International Journal of Greenhouse Gas Control* 16S, S5-S14.
- Johnson, J.W., Mayer, B., Shevalier, M., Perkins, E., Talman, S., Kotzer, T., Hawkes, C., Butler, S., Luo, M., Er, V., Ramirez, A., Carroll, S., Wolery, T., McNab, W., Hao, Y., Carle, S., Jones, D., Beaubien, S., and Le Pierres, K., 2011. Geochemical assessment of isolation performance during 10 years of CO₂ EOR at Weyburn. *Energy Procedia* 4, 3658-3665.
- Kharaka, Y. K., Gunter, W., Aggarwal, P. K., Perkins, E. H. and De Braal, J. D., 1988. SOLMINEQ88: a computer programme for geochemical modelling of water-rock reactions. *USGS Water Resources Investigation Report* 88-4227.

- Kharaka, Y., Cole, D.R., Hovorka, S.D., Gunter, W.D., Knauss, K.G., Freifeld, B.M., 2006 Gas-water-rock interactions in Frio Formation following CO₂ injection: Implications for the storage of greenhouse gases in sedimentary basins. *Geology* 34, 577-580.
- Lasaga, A.C., 1984. Chemical kinetics of water-rock interactions. *Journal of Geophysical Research*. 89, 4009-4025.
- Matter, J M., Martin S., Snæbjörnsdóttir, S. Ó., Oelkers, E.H., Gislason S. R., Aradóttir, E. S., Sigfusson, B., Gunnarsson, I., Sigurdardóttir, H., Gunnlaugsson, E., Axelsson, G., Alfredsson, H.A., Wolff-Boenisch, D., Mesfin, K., D. Fernandez de la Reguera Taya, Hall, J., Dideriksen, K., and Broecker, W.S. 2016. Rapid carbon mineralization for permanent disposal of anthropogenic carbon dioxide emissions. *Science* 10, 1312-1314.
- Mayer, B., Shevalier, M., Nightingale, M., Kwon, J-S., Johnson, G., Raistrick, M., Hutcheon, I., and Perkins, E., 2013. Tracing the movement and the fate of injected CO₂ at the IEA GHG Weyburn-Midale CO₂ Monitoring and Storage project (Saskatchewan, Canada) using carbon isotope ratios. *International Journal of Greenhouse Gas Control* 16, S177-S184.
- Mungan, N., 1981. Carbon dioxide flooding fundamentals. *Journal of Canadian Petroleum Technology* 20, 87-92.
- Omotoso, O., McCarty, D.K., Hillier, S., Kleeberg, R., 2006. Some successful approaches to quantitative mineral analysis as revealed by the 3rd Reynolds Cup contest. *Clays and Clay Minerals* 54, 748-760.
- Palandri, J.L., and Kharaka, Y.K., 2004. A Compilation of Rate Parameters of Water-Mineral Interaction Kinetics for Application to Geochemical Modeling. U.S. Geological Survey Open File Report 2004-1068, p. 74.
- Perez, R.J., Shevalier, M., Hutcheon, I., Mayer, B., 2006. A model for partitioning gases among brines and hydrocarbons in oil reservoirs: Examples from the IEA-GHG Weyburn CO₂ Monitoring and Storage Project, Saskatchewan, Canada. *Journal of Geochemical Exploration* 89, 326-330.
- Petroleum Technology Research Centre, 2014. **What Happens When CO₂ is Stored Underground? Q&A from the IEAGHG Weyburn-Midale CO₂ Monitoring and Storage Project. Global Carbon Capture and Storage Institute Limited, Melbourne. 51 pages.**
- Qing, H., Nimegeers, A.R., 2008. Lithofacies and depositional history of Midale carbonate-evaporite cycles in a Mississippian ramp setting, Steelman-Bienfait area, southeastern Saskatchewan, Canada. *Bulletin of Canadian Petroleum Geology* 56, 209-232.
- Raistrick, M., Mayer, B., Shevalier, M., Perez, R., Hutcheon, I., Perkins, E.H., Gunter, W.D., 2006. Using chemical and isotopic data to quantify ionic trapping of carbon dioxide in oilfield brines. *Environmental Science and Technology* 40, 6744-6749.
- Shevalier, M., Nightingale, M., Mayer, B., Hutcheon, I., Durocher, K., Perkins, E., 2013. Brine geochemistry changes induced by CO₂ injection observed over a 10 year period in the Weyburn oil field. *International Journal of Greenhouse Gas Control* 16S, S160-S176.
- Srivastava, R.K., Huang, S.S. and Dong. M., 2000. Laboratory Investigation of Weyburn CO₂ Miscible Flooding. *Journal of Canadian Petroleum Technology* 39, 41-51.
- Srivastava, R.K., Huang, S.S. 1997. Laboratory investigation of Weyburn CO₂ miscible flooding. *7th Saskatchewan Petroleum Conference*. Regina, 1997.
- Steefel, C.I., and Lasaga, A.C., 1994. A coupled model for transport of multiple chemical species and kinetic precipitation/dissolution reactions with application to reactive flow in a single phase hydrothermal system. *American Journal of Science* 294, 529-592.
- Verma, M.K. 2015. Fundamentals of Carbon Dioxide-Enhanced Oil Recovery (CO₂-EOR)—A Supporting Document of the Assessment Methodology for Hydrocarbon Recovery Using CO₂-EOR Associated with Carbon Sequestration. Open-File, U.S. Department of the Interior, United States Geological Survey, USGS, 2015, p. 19.

- White, D.J. and Johnson, J.W. 2009. Integrated geophysical and geochemical research programs of the IEA GHG Weyburn-Midale CO₂ monitoring and storage project. *Energy Procedia* 1, 2349-2356.
- White, D.J., Hirsche, K., Davis, T., Hutcheon, I., Adair, R., Burrowes, G., Graham, S., Bencini, R., Majer, E., Maxwell, S.C. 2004., Theme 2: prediction, monitoring, and verification of CO₂ movements." Edited by M., Monea, M. (Eds.), In: Wilson. *IEA GHG Wey-burn CO₂ Monitoring and Storage Project Summary Report 2000–2004*. Regina: Petroleum Technology Research Centre. 73-148.
- Wilson, M., Monea, M., 2004. IEA GHG Weyburn CO₂ Monitoring and Storage Project Summary Report 2000–2004. Petroleum Technology Research Centre, Regina, Canada. p. 273.
- Worden, R.H., 2006. Dawsonite cement in the Triassic Lam Formation, Shabwa Basin, Yemen: A natural analogue for a potential mineral product of subsurface CO₂ storage for greenhouse gas reduction. *Marine and Petroleum Geology*, 23, 61-77.
- Xu., T., Apps, J.A., and Pruess, K., 2004. Numerical simulation of CO₂ disposal by mineral trapping in deep aquifers. *Applied Geochemistry* 19, 917-936.
- Xu, T., Kharaka, Y., Doughty, C., Freifeld, B. and Daley, T.M., 2010. Reactive transport modeling to study changes in water chemistry induced by CO₂ injection at the Frio-I brine pilot. *Chemical Geology* 271, 153-164.
- Yang, D., Gu, Y., Tontiwachwuthikul, P. 2008. Wettability determination of the reservoir brine-reservoir rock system with dissolution of CO₂ at high pressures and elevated temperatures. *Energy and Fuels* 22, 504-509.
- Yuo, P., Vahapcan, E., Freitag, N., Huang, S., 2013. Recharacterizing evolving fluid and PVT properties of Weyburn oil–CO₂ system. *International Journal of Greenhouse Gas Control* 16S, S226-S235.

FIGURE CAPTIONS

Figure 1. Location map of the Weyburn field in southern Saskatchewan, Canada. The phase 1A area is shown in the shaded area of the inset. The inset map of the Weyburn field is contoured for values of oil API gravity. W1, W2 and W3 are the locations of wells with measured solubility of CO₂ in oil from Srivastava et al. (2000).

Figure 2. Representative petrography and mineral abundance data for the Midale Marly M0 flow unit. Thin section field of view is 500 µm. Scale bar on the SEM photomicrograph is 10 µm.

Figure 3. Representative petrography and mineral abundance data for the Midale Vuggy V2 flow unit. Thin section field of view is 500 µm. Scale bar on the SEM photomicrograph is 100 µm.

Figure 4. Equilibrium reaction path simulation of addition of CO₂ to M0 flow unit at 60°C and 1 bar.

Figure 5. Kinetic reaction path simulation of addition of CO₂ to M0 flow unit at 60°C and 1 bar.

Figure 6. Mineral storage of CO₂ by flow unit for equilibrium and kinetic models. “Eum” refers to equilibrium models, “Kin” refers to kinetic models “Hi” is high, and “Lo” is low.

Figure 7. Kinetic simulation of M0 flow unit for high TDS saline formation water at 60°C and starting $f\text{CO}_2 = 85$ bar, showing the evolution of mineral amounts at the end of injection over 5000 years. Red lines represent the difference in mineral amounts. The blue line is the change in CO₂ fugacity. Note that time 0 is after 50 years of CO₂ injection and no additional CO₂ is added during the simulation.

Figure 8. The stability of dawsonite at 60°C and 1 bar. (a) The activity of aqueous SiO₂ is set by equilibrium with chalcedony. Solid boundaries represent stability of dawsonite relative to albite. Dashed boundaries represent stability relative to analcime. (b) Dotted lines show analcime stability with dawsonite suppressed. Dashed ($\log f\text{CO}_2 = -0.5$) boundaries and solid boundaries ($\log f\text{CO}_2 = 1.0$) show the stability of dawsonite relative to albite, kaolinite and Na-beidellite (smectite). The range of $\log f\text{CO}_2$ at Weyburn is between -0.5 and 1.0.

Figure 9. Storage of CO₂ in supercritical fluid, saline formation water, minerals and oil at the end of 50 years of injection at the Phase 1A area in Weyburn.

Acknowledgements

The International Energy Agency Weyburn–Midale project is coordinated by the Petroleum Technology Research Center of Regina, Saskatchewan, in collaboration with Cenovus (the operator of the Weyburn oilfield) and Apache Corporation (the operator of the Midale oilfield). Financial sponsorship of the project was provided by Natural Resources Canada, the U.S. Department of Energy, Alberta Energy Research Institute, Saskatchewan Industry and Resources, the European Community and ten industrial sponsors.

We gratefully acknowledge the assistance of several individuals and organizations. Steve Whittaker, Chris Gilboy, and Erik Nickel of Saskatchewan Industry and Resources (SIR) provided help in obtaining core samples. Ian DeWolfe, (University of Calgary) assisted in sampling and sample preparation. Geoff Burrowes (Cenovus) took time to familiarize KD with typical Weyburn Unit core. Geoff Burrowes, Trevor Westman and Stan Wright (Cenovus) provided estimates of total pore volume, fluid saturations, flow unit interval information for cored wells and petrophysical data, as well as patient assistance with a range of other requests for data. Analytical assistance from Rob Marr and Mickey Horvath (U of Calgary), Pam King and Roger Mason (Memorial University of Newfoundland), is greatly appreciated. Discussion with Bill Gunter and Dirk Kirste helped to clarify the constraints on equilibrium and kinetic reaction path models. Reviewers provided insightful comments that greatly improved the final manuscript.